THE ELASTIC SCATTERING OF PROTONS BY Li^7

Thesis by

William D. Warters

In Partial Fulfillment of the Requirements

for the Degree of

Doctor of Philosophy

California Institute of Technology

Pasadena, California

1953

ACKNOWLEDGEMENTS

It is a pleasure to acknowledge the active assistance and many helpful suggestions of Professor W. A. Fowler in connection with this work. I am also indebted to Professors C. C. Lauritsen and T. Lauritsen for valuable aid and advice, and to Professor R. F. Christy and Mr. D. A. Liberman for enlightening discussions of the theoretical analysis of the data. I wish to thank Mr. E. A. Milne for many hours of help in testing the apparatus and taking the data.

The construction of the variable angle spectrometer mounting resulted from the joint efforts of several people. In addition to those mentioned above, Mr. V. F. Ehrgott of the Kellogg Laboratory drafting department and Mr. G. Fastle and Mr. L. J. Gilliland of the machine shop contributed greatly.

I wish to express my gratitude to the National Science Foundation for a predoctoral fellowship received during the academic year 1952 - 1953. The experimental work described in this thesis was supported by the joint program of the Office of Naval Research and the Atomic Energy Commission.

Above all, I am grateful to my wife Margot for her help and patience during the completion of this work.

ABSTRACT

A double focusing magnetic proton spectrometer has been so mounted as to permit observations over a continuous range of scattering angles from 0 to 160 degrees. With this instrument, the cross section for the reaction Li^7 (pp) has been measured over the proton energy range 360 - 1400 kev. Measurements were made at scattering angles of 50, 70, 89.2, 110, 130, 143.4 and 160 degrees in the center-of-mass system. Anomalous scattering was observed near 441 kev, the resonance energy for the reaction Li^7 (p γ), and near 1030 kev, the resonance energy for the reaction Li^7 (pp'). Analysis of the results near 441 kev indicates a state in Be^8 with J = 1, even parity, formed by p-wave protons, while the analysis near 1030 kev indicates a state in Be^8 with J = 1, odd parity, formed by s-wave protons. The relative stopping cross section for protons in lithium has also been measured from 200 - 1300 kev.

TABLE OF CONTENTS

INTRODUCTION

The transmutation of Li^7 by protons has been of interest for many years. In 1932 Cockroft and Walton[1] first observed alpha particles from the reaction Li^7 (pα). Gamma rays from the well-known 441 kev resonance in the reaction Li^7 (p γ) were observed in 1934 by Lauritsen and Crane[2]; and the width and position of the resonance were measured accurately by Hafstad and Tuve[3] in 1935. In 1939 Creutz[4] studied the protons elastically scattered by lithium at an angle of 156° over the incident proton energy range 272 - 586 kev. He found a marked anomaly in the scattering at 440 kev and concluded that the gamma radiation from Li + p at that energy arose from a virtual level in Be^8.

Accurate measurements of the resonance energies of the reactions Li^7 (p γ) and Li^7 (pp') have been made by Fowler and Lauritsen[5], who give 441.4 ± 0.5 kev for the Li^7 (p γ) resonance and 1030 ± 5 kev for the Li^7 (pp') resonance. Hunt [6] has recently found 441.5 ± 0.5 kev for the resonance in Li^7 (p γ) using an absolute electrostatic analyzer. The angular distribution of the gamma radiation near this resonance has been determined by Devons and Hine[7] who concluded that the excited state in Be^8 has J = 1, odd parity, and is formed by s-wave protons.

A study of the elastic scattering of protons from Li^7 can be expected to provide additional information which will aid in the determination of the nature of the highly excited states of Be^8.

One expects to find anomalies in the scattering corresponding to the resonances in the reactions Li^7 (p γ) and Li^7 (pp') with perhaps a small effect due to the broad resonance in the reaction Li^7 (pα) at 3 Mev. The cross section for the reaction Li^7 (pp) has been measured by Brown, et al.[8], at 89.2 and 143.4 degrees in the center-of-mass system, over the incident proton energy range 300 - 1300 kev. They found anomalies near 441 kev and near 1030 kev. An analysis of their results near 441 kev by Cohen[9] indicated that the state in Be^8 has J = 1, even parity, and is formed by p-wave protons. This result is seen to be in disagreement with the results of Devons and Hine.

This inconsistency in experimental results indicated that more complete experiments should be performed. Equipment has therefore been constructed in the Kellogg Radiation Laboratory to study the angular distribution of charged nuclear reaction products. This thesis describes measurements of the cross section for the reaction Li^7 (pp) at center-of-mass angles of 50, 70, 89.2, 110, 130, 143.4 and 160 degrees for incident proton energies in the range 360 - 1400 kev. It is believed that sufficient data are provided to permit unique assignments for the 17.62 Mev and 18.14 Mev states in Be^8, which correspond to the observed anomalies in the scattering at proton energies near 441 kev and 1030 kev, respectively.

During these experiments it was found desirable to measure the stopping cross section of protons in lithium. A relative determination was performed over the energy range 200 - 1300 kev, and the results are included in this thesis.

II. APPARATUS

The 1.7 Mv electrostatic generator of the Kellogg Radiation Laboratory provided the proton beam used in this experiment. The beam was rendered mono-energetic to 0.05 per cent by an 80 - degree electrostatic analyzer of 1 meter radius and 1 millimeter entrance and exit slits. The scattered protons were analyzed by a 10 1/2 inch double-focusing proton spectrometer after mounting the spectrometer on a pivoted support which allows measurements to be made at any angle from 0 to 160 degrees. The protons accepted by the spectrometer were counted by the scintillation counter and pulse amplifier built by A. V. Tollestrup[11]. The general arrangement of the apparatus is shown in Figure 1A.

1. Construction of the Variable Angle Spectrometer.

The variable angle spectrometer is so constructed that the entire spectrometer and the bottom half of the target chamber rotate about a vertical axis which passes through the object focal point of the spectrometer. The top half of the target chamber is connected to the entrance tube for the incident beam from the electrostatic analyzer, and remains stationary. The movable joint between the halves is in the horizontal plane which passes through the object focal point of the spectrometer; and the vacuum seal between the halves is provided by an "O"-ring contained in the joint. The target is held at the focal point of the spectrometer

from the top half of the chamber. The proton beam therefore enters the chamber through the top half, strikes the target, and leaves through the bottom half. This construction is illustrated in Figure 1B. Clearance of the movable joint is provided by directing the incident beam downward exactly 10 degrees from horizontal with the 80-degree electrostatic analyzer. Consequently, as the spectrometer is swung through 180 degrees, the accepted scattering angle varies through 160 degrees. The angle through which the spectrometer has been turned is read with an attached protractor and vernier, and the corresponding scattering angle is then calculated from the known geometry.

Before the construction of this equipment, measurements were made on the gap and fringing fields of the spectrometer magnet, using a flip coil and Grassot fluxmeter. Accurate location of the object focal point was obviously necessary, and since the magnet was known to exhibit a strong fringing field it was feared that the radial position of this point might vary with field strength. The measurements were also valuable for determining the focusing characteristics of the spectrometer. Tests were made using both a brass entrance tube to the spectrometer and an iron entrance tube which was designed to shield the entering protons from the fringing field. With no shielding it was found that the fringing field was so strong that the equilibrium path of the spectrometer was bent 11.8 degrees in the 12 inches between target and pole faces, but that the ratio of the fringing field strength to the

gap field strength at the equilibrium orbit remained constant at all points over the entire operating range of the spectrometer. This indicated that the magnetic circuit of the instrument did not saturate in the pole pieces. The iron entrance tube reduced the curvature of the entering beam, but was found to become saturated and thereby to destroy the constant field ratio. The apparatus was therefore constructed with no shielding. The relative field strength along the equilibrium path for this case is shown in Figure 2. Measurements of the radial variation of the gap field of the magnet were also made. The criterion for double-focusing, with axial and radial focal lengths equal, is that the field vary as r^{-n}, where $n = 1/2$. The results of this measurement indicate that for this spectrometer $n = 0.50 \pm 0.02$ over the range $r = 10.5 \pm 0.8$ inches (Figure 3).

The focusing characteristics of the spectrometer were also measured directly with the proton beam after the construction was completed. The spectrometer was set at zero degrees so that the incident beam passed directly into the instrument. To make the beam diverge from the object focal point, several kilovolts A.C. were applied across two parallel plates which were mounted at the target position in such a way that the beam passed between them. The axial and radial image focal points were then determined by observing the beam at the image side of the spectrometer on a movable quartz disk. The axial image point was found to be 4 3/16 inches and the radial point 3 3/4 inches from the magnet pole face.

Thus the instrument is non-astigmatic for all practical purposes. The separation of the focal points indicates that the field parameter n is actually 0.495.

The strong fringing field of the spectrometer was found to interfere with the incident beam from the electrostatic analyzer when the spectrometer was near the 160-degree position. The analyzer casing was therefore built of steel, and a steel lining was put inside the entrance tube to the target chamber. This construction made the effect negligible.

The constant proportionality of the spectrometer fringing field to the equilibrium orbit field was a great advantage as it meant that the fluxmeter used to measure and control the field during experiments did not have to be mounted at the equilibrium orbit. It was actually mounted outside of the vacuum chamber near the edge of the gap, where its calibration has been found to remain constant over the operating range of the spectrometer.

The fluxmeter used to measure the spectrometer field was built by Mr. E. A. Milne[12]. A control circuit for the field was also built, which operates on an error signal from the fluxmeter. The control drives an amplidyne which is connected into the field circuit of the generator which supplies the spectrometer. With this device, the spectrometer field is held at a given setting to within 0.05 per cent.

2. Methods and Uncertainties of Calibrations.

The 80-degree electrostatic analyzer was calibrated from observations of the gamma radiation from the resonances in the reactions Li^7 (p γ) at 441.5 kev[6] and Al^{27} (p γ) at 993.3 kev[13]. The kinetic energy of a particle with charge Z traveling through the electrostatic analyzer is, non-relativistically, proportional to the potential across the analyzer plates. It is therefore given by

$$E = C_E Z E_{pot}, \tag{2.1}$$

where E_{pot} is the reading of a potentiometer across part of the analyzer plate resistor stacks, and C_E is a constant determined by the calibration. The energy of the beam when it strikes the target is less than this, however, because the target is raised to a potential V_G to suppress the escape of secondary electrons. The actual bombarding energy is therefore

$$E_{1B} = C_E Z E_{pot} - V_G Z. \tag{2.2}$$

In these experiments V_G was 300 volts; so this was a small correction. It was, however, included. The correction to E_{1B} for relativistic effects is 0.075 per cent for E_{1B} = 1400 kev, and correspondingly less for lower energies; so it was neglected. The determination of C_E was repeated at different times during the course of these experiments, and its value was found to vary less than 0.1 per cent.

The energy calibration of the magnetic spectrometer was performed by studying the protons elastically scattered from copper, gold, aluminum and lithium using the electrostatic analyzer calibration and the conservation laws of energy and momentum. The momentum of a particle with charge Z traveling through the magnetic spectrometer is directly proportional to the magnetic induction B at the equilibrium orbit. The magnetic induction is measured with a moving coil, balanced torque fluxmeter; so the current flowing through the coil at balance varies inversely with B. The kinetic energy of a particle which passes through the spectrometer is therefore given non-relativistically by

$$E = \frac{C_I}{M} \frac{Z^2}{I_{pot}^2} \tag{2.3}$$

where M is the mass of the particle, I_{pot} is the reading of a potentiometer across a resistor in series with the fluxmeter coil and C_I is a constant. The ratio C_I/M was determined for protons by the calibration. For accuracy one must again include the effect of the target guard potential; so that the energy which a particle passingthrough the spectrometer had when it left the target is

$$E_{2o} = \frac{C_I}{M} \frac{Z^2}{I_{pot}^2} - V_G Z. \tag{2.4}$$

The relativistic correction is again less than 0.075 per cent. The determination of C_I/M was performed with the spectrometer at 90 degrees

and was repeated several times during the course of the experiments. Its value was found to remain constant to within 0.2 per cent.

The scattering angle accepted by the spectrometer is calculated from the spectrometer angle setting, assuming the proton beams entering and leaving the target chamber are exactly 10 degrees from horizontal. The zero scattering angle is set by passing the direct beam from the analyzer exactly through the center of the spectrometer and setting the protractor vernier to zero degrees. The 10-degree beam angles were carefully checked during construction of the apparatus; so the uncertainty in the scattering angles is believed to be less than 0.1 degree.

The radial exit slits of the spectrometer, which determine the resolution of the instrument, were measured with a comparator to 0.0001 inches. This corresponds to an uncertainty of 0.7 per cent for the smallest slit. The solid angle apertures and the counter efficiency were calibrated together by studying the protons elastically scattered from copper, assuming pure Coulomb scattering. A previous test on copper using very small apertures measured geometrically had indicated that the Coulomb cross section was valid. For the calibration calculations it was necessary to know the stopping cross section for protons in copper, and the results of Warshaw[14] were used. The stopping cross section of copper and the assumption of pure Coulomb scattering introduce a probable error of about 5 per cent in the absolute magnitude of the solid angle calibration.

It was thought that perhaps fringing fields, second order focusing effects, or slight misalignments might change the spectrometer energy or solid angle calibration with the scattering angle, or might make the solid angle calibration depend upon the size of the spectrometer exit slit. The energy calibration was therefore checked at six different scattering angles and found to remain constant within a probable error of 0.2 per cent. The solid angle calibration was repeated for each entrance aperture and exit slit combination at 90 and 160 degrees and for one combination at ten different angles between 30 and 160 degrees. The maximum probable error found for any solid angle value was 2 per cent.

The current integrator capacitances were measured by J. W. Reeds to 1 per cent. The integrator firing voltage was read each day to 0.4 per cent. The resolving time of the counting system was measured, and a counting rate correction curve was drawn. The leakage rate of the integrator capacitors was measured daily, and the number of counts was also corrected for this effect. These corrections never totaled more than a few per cent.

3. Preparation of Targets.

The bottom of the target chamber was fitted with an evaporating oven for making targets under vacuum. The targets consisted of layers of natural lithium (92.5 per cent Li^7) deposited on a copper backing. The layers were made very thick as the high resolution of the spectrometer gives the instrument the

ability to isolate a thin lamina at any desired depth in the target material.

The target was held by a mounting equipped with a protractor, with which the angle between the target normal and the incident beam could be set at a given value to within 0.25 degrees. The corresponding uncertainty in the scattering data is less than one per cent. The target mounting also had a vertical adjustment with ten accurately reproducible target positions. This adjustment enabled one to make full use of each target, and to compare the conditions of various parts of each target.

Much time was spent during the course of the experiments in the attempt to obtain satisfactory targets. The requirements were a shiny mirror surface, no internal contaminations, and a minimum of surface layer contamination. Contaminations were determined with the spectrometer by running a momentum spectrum or "profile" of protons scattered by the target. The target chamber was pumped directly by an auxiliary pump equipped with a liquid air trap, and another liquid air trap was installed which ran the length of the target chamber, passing about 2 centimeters from the target. With this arrangement vacua of about 5×10^{-6} mm. Hg were maintained in the chamber during the experiments. By carefully outgassing the lithium furnace for several hours before making a target it was found possible to keep the pressure below 10^{-5} mm. Hg even when evaporating lithium. Nevertheless it was found necessary to deposit the lithium as rapidly as possible in order that the

target not be slightly contaminated throughout with oxygen due to continuous oxidation of the material as it was deposited. By trial and error a depositing rate was determined which gave a target with no detectable internal contamination and a true mirror surface. However, after such a target was made the surface slowly oxidized even though a high vacuum was maintained; so targets were not kept for longer than one day even if they were not used. Bombardment of a target with the proton beam deposited surface contamination layers of carbon and oxygen; therefore the condition of the target was checked frequently during runs and fresh targets were prepared whenever needed. Heating the target was found to practically eliminate the carbon contamination, but it also made the lithium surface oxidize at a much greater rate; so the targets were used unheated.

III. THE CONVERSION OF SCATTERING DATA INTO PHYSICAL RESULTS

1. The General Cross Section Formula.

In any nuclear reaction the total cross section for the reaction is defined as

$$\sigma = \frac{\text{Total yield of reaction}}{\text{Disintegrable nuclei per unit area along incident beam}}$$

where the total yield is the number of disintegrations per incident particle, and a disintegration is broadly defined as the occurrence of the process of interest. In general, the yield will depend upon the kinetic energy of the particles in the incident beam (for our purposes we may assume the target nuclei are at rest in the laboratory system), and will have a non-isotropic distribution about the direction of the incident beam. If for each disintegration exactly one particle of type p is produced among the reaction products, we may define the differential cross section

$$\frac{d\sigma(E,\theta)}{d\Omega} = \frac{y_p(E,\theta)}{Nt} \qquad (3.1)$$

where $y_p(E,\theta)$ is the yield of particle p per unit solid angle at angle θ with the incident beam, N is the number of disintegrable nuclei per unit volume in the target material and t is the thickness of the target along the line of the incident beam. E is the energy of the incident particles when traversing t. Since the particles lose energy as they travel through the target material, E is known

only within a finite range which depends on the magnitude of t.

In a detector sensitive to product p of the reaction, the number of particles recorded is

$$n_p = n \Omega y_p(E,\theta) \qquad (3.2)$$

where n is the number of incident particles, Ω is the solid angle subtended by the detector at the target, and θ is the angle between the direction of the incident beam and the line of flight of the detected particles. Thus

$$\frac{d\sigma(E,\theta)}{d\Omega} = \frac{1}{\Omega} \frac{n_p(E,\theta)}{n} \frac{1}{Nt} . \qquad (3.3)$$

These quantities are all measurable. The solid angle may be determined geometrically or by calibrating on a reaction where everything else is known. If each incident particle carries charge Ze the total number n may be determined by allowing the beam to charge a capacitance C to potential V, so

$$n = CV/Ze. \qquad (3.4)$$

n_p is the number of counts recorded by the detector, and N is easily calculated from the chemical formula, density, and isotopic abundances of the target. This leaves the target thickness t to be determined, and it is the measurement of this quantity which usually presents the greatest uncertainty.

It should be emphasized that n_p represents the number of

particles coming from exactly a thickness t of the target material. Since particles lose an amount of energy in traveling through the target according to the distance traveled in the target, the reaction products from a target of finite thickness are found in a finite range Δ of energy or momentum. If the detector used is selective in energy or momentum and accepts particles only over a spread δ, then the detector itself determines the thickness t of the effective target if $\delta < \Delta$. This condition enables one to use a thick target and to calculate the actual reaction thickness t from the properties of the detector.

2. Detection of Charged Particles with the Variable Angle Spectrometer.

As a detector of charged particles the magnetic spectometer is particularly suitable. It has high resolution and therefore enables one to select a very thin target lamina from a thick layer of target material. The effective target thickness t and the bombarding energy E are then determined as follows.

Let us assume a reaction of the form A(bp)B where bombarding particle b reacts with target nucleus A producing particle p and residual nucleus B. A beam of particles b is incident with energy E_{1B} on the target at angle θ_1 (Figure 4). The spectrometer is set to detect particles p leaving the target with energy E_{2o} at angle θ_2 (θ_{LAB} with the incident beam). The incident beam penetrates the target, losing energy, and at any point

a reaction may occur. If the masses of all participating nuclei are known one can calculate from the conservation laws of energy and momentum the quantity $E_2/E_1 = \alpha = \alpha(E_1, \theta_{LAB}, M_A, M_B, M_p, M_b)$ where E_1 is the energy of b immediately before the reaction and E_2 is the energy of p immediately after.

It is necessary to introduce the stopping cross section $\varepsilon(E) = 1/N_s(dE/dx)$ where dE/dx is the energy loss of a given particle per unit length of travel through the target material and is a function of the energy E of the particle, and where N_s is the number of effective stopping atoms per unit volume of the target. $\varepsilon(E)$ may be determined experimentally by direct measurements or from range-energy results.

The energy of a particle b which has penetrated the target to depth x measured perpendicular to the target surface is therefore

$$E_1 = E_{1B} - \frac{x}{\cos \theta_1} N_s \varepsilon_b(\bar{E}_1) \qquad (3.5)$$

where $\bar{E}_1$ is some intermediate energy between E_1 and E_{1B}. In practice the quantity $\frac{E_1}{E_{1B} - E_1}$ is of the order of the resolution of the spectrometer, and it can be shown that under such conditions one may take $\bar{E}_1 = E_1$ in the preceding equation with negligible loss of accuracy. Therefore if a reaction takes place at depth x in the target, a product p produced at angle θ_{LAB} will have energy

$$E_2 = \alpha E_1 = \alpha E_{1B} - \alpha \frac{xN_s}{\cos \theta_1} \varepsilon_b(E_1).$$

It will again lose energy in escaping from depth x in the target, and will enter the spectrometer with energy

$$E_{2o}' = E_2 - \frac{x}{\cos \theta_2} N_s \varepsilon_p(E_2)$$

$$= \alpha E_{1B} - xN_s \left[\frac{\alpha}{\cos \theta_1} \varepsilon_b(E_1) + \frac{1}{\cos \theta_2} \varepsilon_p(E_2) \right] . \tag{3.6}$$

For some depth x_o, E_{2o}' will equal the spectrometer energy setting E_{2o}, and the particle will travel through the spectrometer and be counted. We may then solve equations 3.5 and 3.6 for E_1, the reaction energy, finding

$$E_1 = \frac{\eta E_{1B} + E_{2o}}{\alpha + \eta} \tag{3.7}$$

where

$$\eta = \frac{\cos \theta_1 \ \varepsilon_p(\alpha E_1)}{\cos \theta_2 \ \varepsilon_b(E_1)} . \tag{3.8}$$

In practice the target is usually set so that $\theta_1 = \theta_2$, making $\cos \theta_1 / \cos \theta_2 = 1$.

To find the target thickness selected by the spectrometer we differentiate 3.6, with $E_{2o}' = E_{2o}$, finding

$$dE_{2o} = - \frac{dx \ N_s}{\cos \theta_1} \ \varepsilon_b(E_1)(\alpha + \eta).$$

If $|dE_{2o}|$ is equal to δE_{2o}, the energy spread accepted by the spectrometer, then the target thickness selected is just $dx/\cos \theta_1$,

so that

$$\frac{1}{t} = \frac{N_s}{\delta E_{2o}} (a + \eta)\ \varepsilon_b(E_1). \qquad (3.9)$$

We can express this in terms of the resolution calculated from the width of the detector window, which for a magnetic spectrometer is given by

$$R = \frac{P}{\delta P} = 2 \frac{E_{2o}}{\delta E_{2o}}$$

$$= 2(1 + M) \frac{r_o}{\delta r}$$

where M is the magnification, r_o the equilibrium orbit radius and δr the radial width of the exit slit of the instrument. In terms of the resolution, equation 3.9 becomes

$$\frac{1}{t} = \frac{R}{2E_{2o}} N_s(a + \eta)\ \varepsilon_b(E_1)$$

$$= (1 + M) \frac{r_o}{\delta r} \quad \frac{(a + \eta)}{E_{2o}} N_s\ \varepsilon_b(E_1). \qquad (3.10)$$

Introducing equations 3.10 and 3.4 into equation 3.3, our expression for the differential cross section becomes

$$\frac{d\sigma}{d\Omega}(E_1,\theta) = \frac{N_s}{N} \frac{Ze}{CV\Omega} \frac{R}{2E_{2o}} (a + \eta)\ \varepsilon_b(E_1)\ n_p(E_1,\theta) \qquad (3.11)$$

where

$$\alpha = \frac{E_2}{E_1} = \left[\frac{(M_b M_p)^{1/2}}{M_p + M_b} \cos \theta_{LAB} \pm \left(\frac{M_B}{M_P + M_B} \frac{Q}{E_1} + \frac{M_B - M_b}{M_B + M_P} + \frac{M_b M_p}{(M_B + M_P)^2} \cos^2 \theta_{LAB} \right)^{1/2} \right]^2 \qquad (3.12)$$

and

$$Q = (M_{bo} + M_{Ao} - M_{po} - M_{Bo})\, c^2,$$

the subscript o denoting rest mass plus mass equivalent of any excitation. Equation 3.11 is valid in either the laboratory or center-of-mass system, depending on which system is used to express the quantities Ω and θ.

3. Application of General Formulae to Elastic Scattering Experiments.

In applying the above general formulae to the experiments on the elastic scattering of protons from Li^7 described in this thesis, the following simplifications were made.

The target and residual nuclei are identical in an elastic scattering phenomenon, as are the bombarding and emitted particles b and p; so in this case $Q = 0$, and equation 3.12 reduces to

$$\alpha = \frac{E_2}{E_1} = \left[\frac{m}{m + M} \cos \theta_{LAB} \pm \frac{1}{m + M} (M^2 - m^2 \sin^2 \theta_{LAB})^{1/2} \right]^2 \qquad (3.12a)$$

where m is the mass of the proton and M the mass of the scattering

nucleus. For any given elastic scattering process, therefore, α depends only upon the scattering angle.

The depth in the target of the actual target lamina from which data are taken is of some importance. If the lamina is too deep, straggling becomes very large and the energy resolution of the data is destroyed. If the lamina is too near the surface the exit window of the spectrometer may not be filled, rendering equation 3.11 invalid. The compromise followed in this experiment was to operate with the lamina beneath the surface a distance which was a constant small multiple of its own thickness. Thus as the proton bombarding energy was varied over the investigated range, the setting of the spectrometer was also varied in such a way as to fulfill this criterion. For such a "following curve", using equations 3.6 and 3.9 for the depth in the target $x/\cos\theta_1$ and the lamina thickness t, the criterion $\frac{x}{\cos\theta_1} = nt$ gives

$$\alpha E_{1B} - E_{2o} = n\,\delta E_{2o} = n\frac{2E_{2o}}{R} \qquad (3.13)$$

or

$$\frac{E_{1B}}{E_{2o}} = \frac{1}{\alpha}\left(1 + \frac{2n}{R}\right) .$$

Introducing the constants of the apparatus from equations 2.2 and 2.4 and ignoring the small target potential corrections we have

$$\frac{C_E}{C_I} E_{pot} I_{pot}^2 = \frac{1}{\alpha}\left(1 + \frac{2n}{R}\right)$$

so that

$$E_{pot}\ I_{pot}^{2} = K.$$

K is designated the "following constant", and depends upon the scattering angle, the constants of the apparatus, the resolution setting of the spectrometer, and the "following depth" n in the target. In this experiment K was held fixed for each angle over the energy range studied, and n was always near 4.

Calculation of E_1 from the experimental settings of E_{1B} and E_{2o} by use of equation 3.7 is complicated by the fact that the quantity η is itself a function of E_1. However, the variation of E_1 with η is small, as is shown by differentiating equation 3.7, substituting 3.13 and using the definition of $\varepsilon(E)$:

$$\frac{dE_1}{d\eta} = \frac{aE_{1B} - E_{2o}}{(a+\eta)^2} = \frac{n\ \xi(E_1)}{a+\eta}$$

where n is the "following depth" of the target and $\xi(E_1)$ is the energy thickness of the target lamina. For these experiments n was about 4 and $(a+\eta)$ near 2; so $dE_1 \sim 2d\eta\ \xi(E_1)$. Therefore one needed to know η only within approximately 0.5 in order to determine E_1 within the uncertainty introduced by the finite target thickness alone. If one assumes an expression for $\varepsilon(E)$ of the form

$$\varepsilon(E) = \frac{C}{E^{(a+bE)}}$$

where the constants C, a and b are determined empirically from a curve for $\varepsilon(E)$, then with $\theta_1 = \theta_2$ equation 3.8 becomes

$$\eta(E) = \frac{\varepsilon(\alpha E)}{\varepsilon(E)} = \left(\frac{1}{\alpha}\right)^{a+bE}.$$

Expanding about some value E_o we obtain

$$\eta(E) = \left(\frac{1}{\alpha}\right)^{a+bE_o} \left[1 + b(E - E_o) \log \frac{1}{\alpha}\right]$$

$$= \eta_a \left(1 + \frac{\Delta \eta(E)}{\eta_a}\right).$$

Thus the error in $\eta(E)$ introduced by using $\eta = \eta_a = \left(\frac{1}{\alpha}\right)^{a+bE_o}$ is $\Delta \eta(E) = \left(\frac{1}{\alpha}\right)^{a+bE_o} b(E - E_o) \log \frac{1}{\alpha}$. For lithium, the stopping cross section $\varepsilon(E)$ is well represented by the above empirical formula over the energy range 200 - 1500 kev if one takes a = 0.60 and b = 0.00012. Since the present experiments were performed over the energy range 400 - 1400 kev, we take E_o = 900 kev, which gives

$$\eta_a = \left(\frac{1}{\alpha}\right)^{0.71}, \qquad \Delta \eta(E) < 0.05$$

over the entire range of angles and energy studied. This is seen to cause an error in the determination of E_1 less than one tenth the energy thickness of the target lamina, which is negligible. η_a was therefore used throughout this work in the calculation of E_1.

IV. THE CROSS SECTION FOR THE REACTION $Li^7(pp)Li^7$.

1. Experimental Results.

The elastic scattering of protons by lithium was studied at scattering angles of 50, 70, 89.2, 110, 130, 143.4 and 160 degrees in the center-of-mass system over the incident proton energy range 360 - 1400 kev. The ratio of the observed cross section to the Rutherford scattering cross section over the proton energy range 360 - 500 kev at the angles studied is shown in Figures 5, 6 and 7. The center-of-mass differential cross section over the energy range 500 - 1400 kev for these angles is shown in Figures 8, 9 and 10. Tables 1 - 7 give the experimental results for the differential cross section and for the ratio to the Rutherford scattering at each energy measured for the various angles. The maxima in the scattering for proton energies near the 441.5 kev $Li^7(p\gamma)$ and the 1030 kev $Li^7(pp')$ resonances are shown in Table 8. The values given in Table 8 include corrections for the resolution effects of the apparatus, while the others do not.

The sources of error and uncertainty in these measurements have been discussed in detail in the preceding sections of this thesis. The total uncertainty in the energy calibration of the apparatus is below 0.5 per cent, and non-linearities and systematic errors are believed to be less than 1 per cent. The probable error in the absolute magnitudes of the various spectrometer solid angle apertures is of the order of 5 per cent, while the uncertainty

between the relative values of different combinations of solid angle aperture, spectrometer exit slit and current integrator capacitance is another 2 per cent. The reproducibility of results, which is affected by errors in settings, target smoothness and contamination, straggling, et cetera, was within 5 per cent. Another 5 per cent uncertainty in the results is introduced by the stopping cross section of protons in lithium. Taking the root mean square of the contributing uncertainties, one finds that the uncertainty in the absolute magnitude of these cross section measurements is of the order of 10 per cent, and in the relative magnitudes is of the order of 5 per cent.

TABLE 1

$Li^7(pp)$, $\theta_{CM} = 50^\circ$. Observed differential cross section in barns/steradian and ratio to Rutherford cross section for incident proton energies in kev.

E_p	σ/σ_R	$d\sigma/d\Omega$	E_p	σ/σ_R	$d\sigma/d\Omega$	E_p	σ/σ_R	$d\sigma/d\Omega$
355	1.12	4.21	458	1.17	2.65	968	.87	.44
365	1.11	3.95	460	1.16	2.61	978	.90	.45
375	1.13	3.82	462	1.16	2.58	988	.96	.467
385	1.11	3.56	464	1.12	2.48	998	.99	.474
395	1.10	3.35	468	1.15	2.50	1007	1.01	.476
399	1.09	3.25	472	1.13	2.42	1017	1.04	.480
403	1.07	3.13	476	1.12	2.35	1027	1.08	.485
407	1.06	3.05	480	1.13	2.34	1037	1.11	.494
411	1.07	3.01	484	1.13	2.30	1047	1.14	.498
415	1.05	2.90	488	1.12	2.24	1057	1.13	.485
419	1.05	2.85	492	1.11	2.18	1067	1.12	.472
423	1.04	2.76	494	1.10	2.15	1077	1.11	.455
427	1.02	2.66	514	1.09	1.97	1087	1.09	.44
429	.99	2.56	533	1.09	1.83	1096	1.09	.43
431	1.00	2.56	553	1.08	1.68	1106	1.07	.42
432	.99	2.53	573	1.07	1.56	1116	1.06	.41
434	1.01	2.56	593	1.08	1.46	1126	1.04	.39
436	1.02	2.56	612	1.07	1.36	1136	1.03	.38
438	1.06	2.63	632	1.05	1.25	1146	1.02	.37
439.4	1.08	2.66	652	1.05	1.16	1156	.98	.35
440.4	1.11	2.72	672	1.03	1.09	1166	1.00	.35
441.3	1.13	2.76	691	1.02	1.02	1176	.96	.33
442.3	1.18	2.86	711	1.02	.96	1185	.96	.32
443.3	1.19	2.89	731	1.01	.90	1205	.94	.31
444.3	1.21	2.91	751	1.00	.84	1225	.91	.29
445.3	1.23	2.95	770	.97	.78	1245	.90	.28
446.3	1.25	2.98	790	.96	.73	1264	.87	.25
447.3	1.24	2.95	810	.95	.69	1284	.82	.24
448.3	1.24	2.93	830	.92	.64	1304	.80	.23
449.2	1.22	2.88	849	.90	.59	1324	.78	.211
450.2	1.21	2.84	869	.88	.56	1343	.76	.200
451.2	1.21	2.83	889	.86	.52	1363	.74	.189
452.2	1.21	2.81	909	.84	.48	1383	.73	.181
454.2	1.19	2.75	928	.84	.46	1403	.70	.169
456	1.18	2.70	948	.84	.45			

TABLE 2

$Li^7(pp)$, $\theta_{CM} = 70^\circ$. Observed differential cross section in barns/steradian and ratio to Rutherford cross section for incident proton energies in kev.

E_p	σ/σ_R	$d\sigma/d\Omega$	E_p	σ/σ_R	$d\sigma/d\Omega$	E_p	σ/σ_R	$d\sigma/d\Omega$
354	1.06	1.19	449	1.34	.93	671	.92	.29
364	1.06	1.12	450	1.32	.91	691	.93	.27
374	1.04	1.04	451	1.29	.89	710	.90	.25
384	1.04	.99	452	1.28	.88	730	.90	.24
394	1.03	.93	453	1.27	.87	750	.86	.214
400	1.03	.90	454	1.21	.82	770	.86	.203
402	1.03	.89	455	1.22	.82	789	.84	.189
404	1.03	.89	456	1.20	.81	809	.85	.182
406	1.04	.89	457	1.20	.80	829	.82	.167
408	1.04	.88	458	1.19	.80	849	.81	.158
410	1.03	.86	459	1.18	.79	868	.82	.153
412	1.03	.85	460	1.18	.78	888	.83	.147
414	1.02	.84	461	1.19	.78	908	.85	.144
416	1.04	.84	462	1.17	.77	928	.91	.148
418	1.02	.82	463	1.14	.75	947	1.00	.156
420	1.03	.82	464	1.14	.74	967	1.16	.174
421	1.02	.81	465	1.14	.74	987	1.30	.187
422	1.02	.80	466	1.14	.73	997	1.39	.196
423	1.03	.81	468	1.12	.72	1007	1.47	.204
424	1.02	.80	470	1.10	.70	1016	1.50	.204
425	1.01	.78	472	1.12	.70	1026	1.51	.201
426	1.03	.80	474	1.09	.68	1036	1.53	.200
427	1.03	.79	476	1.09	.67	1046	1.53	.196
428	1.03	.79	478	1.10	.67	1056	1.51	.190
429	1.03	.79	480	1.11	.67	1066	1.47	.181
430	1.04	.79	482	1.09	.66	1076	1.41	.171
431	1.05	.79	484	1.12	.67	1085	1.37	.163
432	1.04	.78	486	1.09	.65	1105	1.29	.148
433	1.07	.80	488	1.08	.64	1125	1.21	.134
434	1.08	.80	490	1.10	.64	1145	1.14	.122
435	1.09	.81	492	1.09	.63	1164	1.07	.110
436	1.13	.83	493	1.08	.62	1184	1.04	.104
437	1.15	.84	494	1.08	.61	1204	.98	.094
438	1.18	.86	496	1.08	.61	1224	.96	.090
439	1.23	.89	498	1.13	.64	1243	.96	.087
440	1.30	.94	500	1.11	.62	1263	.91	.080
441	1.36	.98	513	1.05	.56	1283	.90	.076
442	1.42	1.02	533	1.04	.51	1303	.88	.072
443	1.45	1.03	553	1.04	.48	1322	.91	.073
444	1.47	1.04	572	1.00	.43	1342	.87	.067
445	1.48	1.04	592	.98	.39	1362	.90	.068
446	1.46	1.03	612	1.00	.37	1382	.91	.067
447	1.42	.99	632	.97	.34			
448	1.40	.98	651	.96	.32			

TABLE 3

$Li^7(pp)$, $\theta_{CM} = 89.2^\circ$. Observed differential cross section in barns/steradian and ratio to Rutherford cross section for incident proton energies in kev.

E_p	σ/σ_R	$d\sigma/d\Omega$	E_p	σ/σ_R	$d\sigma/d\Omega$	E_p	σ/σ_R	$d\sigma/d\Omega$
358	1.03	.50	508	.96	.23	1016	2.12	.128
368	1.03	.48	518	.95	.22	1026	2.11	.126
378	1.01	.44	538	.92	.199	1036	2.09	.122
388	.97	.40	558	.90	.181	1046	2.03	.116
398	1.00	.39	578	.88	.165	1056	1.98	.111
400	1.00	.39	598	.87	.152	1076	1.77	.096
408	.99	.37	617	.85	.139	1096	1.61	.084
418	1.02	.365	637	.83	.128	1115	1.48	.075
428	1.08	.37	657	.83	.120	1135	1.39	.067
433	1.23	.41	677	.80	.109	1155	1.29	.060
434	1.28	.43	697	.79	.102	1175	1.21	.055
435	1.32	.44	717	.76	.092	1195	1.17	.051
436	1.38	.45	737	.77	.088	1215	1.14	.048
437	1.46	.48	757	.75	.082	1235	1.12	.046
438	1.56	.51	777	.75	.078	1255	1.12	.044
439	1.63	.53	797	.74	.073	1275	1.13	.043
440	1.66	.535	817	.75	.070	1295	1.12	.042
441	1.70	.545	837	.77	.069	1315	1.14	.041
442	1.68	.537	857	.80	.068	1335	1.18	.041
443	1.66	.53	876	.86	.070	1354	1.23	.042
444	1.61	.51	896	.93	.072	1374	1.25	.041
448	1.37	.43	916	1.05	.078	1394	1.27	.041
458	1.08	.32	936	1.23	.088			
468	1.01	.29	956	1.44	.098			
478	.97	.27	976	1.74	.114			
488	.96	.25	996	2.00	.126			
498	.96	.24	1006	2.10	.130			

TABLE 4

Li^7 (pp), $\theta_{CM} = 110^\circ$. Observed differential cross section in barns/steradian and ratio to Rutherford cross section for incident proton energies in kev.

E_p	σ/σ_R	$d\sigma/d\Omega$	E_p	σ/σ_R	$d\sigma/d\Omega$	E_p	σ/σ_R	$d\sigma/d\Omega$
359	.99	.26	444	1.64	.28	817	.75	.038
369	.97	.24	445	1.54	.26	837	.82	.039
379	.97	.23	446	1.45	.25	857	.93	.043
388	.98	.22	447	1.34	.225	877	1.03	.045
398	.98	.21	448	1.27	.213	897	1.19	.050
400	.98	.205	450	1.15	.191	917	1.42	.057
402	1.00	.208	452	1.02	.168	937	1.76	.068
404	.99	.206	454	1.00	.164	957	2.16	.079
406	1.01	.206	456	.95	.153	977	2.58	.091
408	.99	.200	458	.95	.153	987	2.79	.096
410	.96	.192	462	.91	.144	997	3.03	.102
412	1.00	.198	466	.89	.139	1007	3.15	.105
414	1.02	.200	470	.89	.137	1017	3.21	.104
416	1.01	.196	474	.85	.128	1026	3.19	.102
418	1.02	.198	478	.84	.124	1036	3.11	.098
420	1.03	.196	482	.88	.128	1046	3.01	.093
422	1.06	.200	486	.85	.121	1056	2.93	.088
424	1.09	.203	490	.84	.117	1076	2.63	.077
426	1.16	.215	494	.84	.115	1096	2.37	.067
428	1.15	.211	498	.85	.112	1116	2.17	.059
429	1.21	.221	518	.83	.104	1136	2.00	.052
430	1.22	.22	538	.81	.094	1156	1.91	.048
431	1.26	.23	558	.78	.085	1176	1.84	.045
432	1.31	.24	578	.76	.077	1196	1.81	.043
433	1.37	.25	598	.74	.070	1216	1.78	.041
434	1.44	.26	518	.73	.064	1236	1.76	.039
435	1.49	.27	638	.73	.060	1256	1.78	.038
436	1.59	.28	658	.69	.054	1276	1.87	.039
437	1.67	.29	678	.69	.051	1296	1.90	.038
438	1.74	.30	698	.67	.046	1316	1.97	.038
439	1.85	.32	717	.67	.044	1335	2.03	.038
440	1.87	.325	737	.68	.042	1355	2.12	.039
441	1.84	.32	757	.69	.041	1375	2.21	.039
442	1.82	.31	777	.69	.039	1395	2.31	.040
443	1.72	.29	797	.73	.039			

TABLE 5

Li^7 (pp), $\theta_{CM} = 130^\circ$. Observed differential cross section in barns/steradian and ratio to Rutherford cross section for incident proton energies in kev.

E_p	σ/σ_R	$d\sigma/d\Omega$	E_p	σ/σ_R	$d\sigma/d\Omega$	E_p	σ/σ_R	$d\sigma/d\Omega$
359	.94	.160	469	.77	.079	960	2.92	.071
369	.97	.160	479	.73	.072	970	3.28	.079
379	.95	.149	489	.72	.068	980	3.64	.085
389	.96	.143	499	.75	.068	990	3.96	.091
399	.95	.134	500	.76	.068	1000	4.25	.096
403	.97	.134	520	.77	.064	1010	4.48	.099
407	.98	.132	540	.76	.059	1020	4.66	.101
411	.96	.128	560	.74	.053	1030	4.59	.097
415	.99	.129	580	.72	.048	1040	4.52	.094
419	1.03	.132	600	.69	.043	1050	4.39	.090
423	1.07	.135	620	.69	.040	1060	4.22	.084
427	1.18	.146	640	.66	.036	1070	4.00	.079
429	1.26	.154	660	.65	.034	1080	3.92	.077
431	1.31	.158	680	.66	.032	1090	3.70	.070
433	1.45	.174	700	.65	.030	1100	3.59	.067
435	1.61	.192	720	.66	.029	1120	3.32	.060
437	1.85	.218	740	.67	.028	1140	3.15	.055
438	1.92	.226	760	.68	.027	1160	3.02	.050
439.3	1.97	.230	780	.72	.027	1180	2.93	.047
440.3	1.99	.231	800	.77	.027	1200	2.92	.046
441.3	1.95	.225	820	.85	.028	1220	2.88	.043
442.3	1.92	.220	840	.92	.029	1240	2.91	.043
443.3	1.75	.200	860	1.06	.032	1260	2.93	.042
445	1.49	.169	880	1.23	.036	1280	3.03	.042
447	1.22	.137	900	1.46	.041	1300	3.10	.041
449	1.12	.125	910	1.63	.044	1320	3.21	.041
453	.91	.100	920	1.83	.049	1340	3.32	.042
457	.80	.086	930	2.05	.053	1360	3.41	.042
461	.82	.087	940	2.34	.060	1380	3.56	.042
465	.79	.082	950	2.63	.066	1400	3.65	.042

TABLE 6

Li^7 (pp), $\theta_{CM} = 143.4^\circ$. Observed differential cross section in barns/steradian and ratio to Rutherford cross section for incident proton energies in kev.

E_p	σ/σ_R	$d\sigma/d\Omega$	E_p	σ/σ_R	$d\sigma/d\Omega$	E_p	σ/σ_R	$d\sigma/d\Omega$
365	.99	.139	448	1.15	.107	618	.58	.029
377	.99	.130	449	1.14	.106	638	.57	.026
389	.96	.119	450	1.13	.104	657	.57	.025
395	.97	.116	451	.91	.084	677	.57	.023
401	.98	.114	452	.90	.082	697	.59	.022
403	.95	.109	453	.89	.081	717	.59	.0214
405	.99	.113	454	.90	.082	737	.60	.0206
407	.97	.109	455	.89	.080	757	.62	.0202
409	1.00	.112	456	.92	.083	777	.67	.0208
411	1.00	.110	457	.94	.084	797	.73	.0215
413	1.02	.112	458	.87	.078	817	.79	.022
415	1.06	.115	459	.79	.070	837	.87	.023
417	1.16	.124	460	.90	.079	857	1.11	.028
419	1.04	.110	461	.83	.073	877	1.17	.029
421	1.08	.114	463	.78	.068	897	1.47	.034
422	1.01	.106	465	.85	.073	917	1.86	.041
423	1.25	.130	467	.76	.065	937	2.36	.050
424	1.15	.119	479	.81	.069	956	3.10	.064
425	1.17	.121	471	.73	.061	976	3.85	.075
426	1.21	.124	473	.77	.064	996	4.57	.086
427	1.16	.119	475	.77	.064	1016	5.04	.091
428	1.16	.118	477	.83	.068	1036	5.12	.089
429	1.36	.138	479	.75	.061	1056	4.85	.081
430	1.31	.132	481	.76	.061	1076	4.47	.072
431	1.34	.135	483	.75	.060	1096	4.14	.064
432	1.39	.139	485	.73	.058	1116	3.91	.059
433	1.46	.145	487	.77	.061	1136	3.72	.054
434	1.50	.149	489	.76	.060	1156	3.54	.049
435	1.61	.159	491	.82	.063	1176	3.53	.048
436	1.74	.171	493	.76	.059	1196	3.47	.045
437	1.86	.182	495	.81	.062	1216	3.54	.045
438	1.97	.192	497	.79	.060	1236	3.53	.043
439	2.08	.202	498	.66	.050	1255	3.63	.043
440	2.12	.205	499	.78	.058	1275	3.71	.043
441	2.12	.204	501	.82	.061	1295	3.79	.042
442	2.02	.193	518	.66	.046	1315	3.87	.042
444	1.73	.164	538	.64	.041	1335	3.97	.042
445	1.58	.149	558	.63	.038	1355	4.13	.042
446	1.41	.132	578	.61	.034	1375	4.20	.041
447	1.29	.121	598	.58	.030	1395	4.41	.042

TABLE 7

$Li^7(pp)$, $\theta_{CM} = 160^\circ$. Observed differential cross section in barns/steradian and ratio to Rutherford cross section for incident proton energies in kev.

E_p	σ/σ_R	$d\sigma/d\Omega$	E_p	σ/σ_R	$d\sigma/d\Omega$	E_p	σ/σ_R	$d\sigma/d\Omega$
373	1.00	.116	471	.87	.063	888	1.67	.034
377	.99	.112	476	.76	.054	898	1.91	.038
381	1.01	.112	481	.80	.056	908	2.10	.041
385	1.02	.111	485	.77	.053	918	2.30	.044
389	1.00	.107	487	.73	.050	928	2.62	.049
393	1.03	.107	489	.78	.053	938	3.03	.056
397	.99	.101	491	.81	.054	948	3.55	.064
401	1.02	.102	493	.76	.050	958	3.94	.069
405	1.03	.101	495	.76	.050	968	4.36	.075
409	1.05	.101	497	.77	.050	978	4.94	.083
413	1.05	.099	499	.77	.050	988	5.56	.092
417	1.11	.103	501	.76	.049	998	5.98	.097
419	1.12	.103	503	.77	.049	1008	6.30	.100
421	1.19	.108	519	.74	.044	1018	6.70	.104
423	1.16	.104	539	.71	.040	1028	6.79	.104
425	1.20	.107	559	.70	.036	1038	6.88	.103
427	1.24	.110	579	.68	.033	1048	6.74	.099
429	1.37	.120	599	.66	.030	1058	6.52	.094
431	1.47	.126	619	.68	.029	1078	6.15	.085
433	1.62	.139	639	.60	.024	1098	5.64	.076
435	1.81	.154	659	.61	.0223	1118	5.40	.070
437	2.03	.171	679	.64	.0224	1138	5.19	.065
438	2.12	.178	699	.62	.0205	1158	5.01	.060
439	2.19	.183	719	.67	.0210	1178	4.99	.058
440	2.26	.188	739	.66	.0195	1198	4.87	.055
441	2.21	.183	759	.70	.0197	1218	4.76	.052
442	2.10	.174	779	.71	.0189	1238	4.89	.051
443	1.95	.160	799	.86	.0218	1258	4.95	.050
445	1.69	.138	809	.90	.0222	1278	4.96	.049
447	1.33	.107	819	.92	.0221	1298	5.20	.050
449	1.12	.090	829	.96	.0226	1318	5.25	.049
451	1.00	.079	839	1.10	.025	1338	5.38	.048
453	.93	.073	849	1.12	.025	1358	5.40	.047
456	.88	.068	858	1.23	.027	1378	5.60	.048
461	.81	.061	868	1.39	.030	1398	5.70	.047
466	.84	.062	878	1.47	.031			

TABLE 8

Maxima of the observed differential cross section and of the ratio to Rutherford cross section near the 441 and 1030 kev anomalies at various center-of-mass angles. These values have been corrected for the effects of resolution in the apparatus. Note that at angles greater than 100 degrees the results near the 1030 kev anomaly indicate spherical symmetry.

	θ_{CM} :	50°	70°	89.2°	110°	130°	143.4°	160°
441 kev	σ/σ_R	1.24	1.49	1.70	1.88	2.00	2.16	2.28
	$d\sigma/d\Omega$	2.97	1.04	.549	.328	.233	.207	.190
1030 kev	σ/σ_R	1.14	1.53	2.12	3.21	4.64	5.15	6.88
	$d\sigma/d\Omega$	.49	.204	.129	.105	.101	.091	.104

2. Discussion of Results.

The cross section for elastic scattering of protons by Li^7 has previously been studied by Brown, Snyder, Fowler and Lauritsen[8] at 89.2 and 143.4 degrees in the center-of-mass system, and by Bashkin and Richards[15] at 166.3 degrees. The work of Brown, et al., was done in the same laboratory as was the present work. The two results at 143.4 degrees are brought within 6 per cent agreement over the entire energy range studied if Brown's data are recalculated using the curve for the stopping cross section of lithium which was measured and used in the present work. However, this correction leaves Brown's results at 89.2 degrees up to 20 per cent lower than the present results. Because of improved experimental techniques, the present results must be assumed to be the better. Bashkin and Richards give ~ 0.08 barn/steradian for the maximim differential cross section near the 1030 kev anomaly at 166.3 degrees. As their uncertainty is 20 per cent, the agreement with the present work is within experimental error.

A theoretical analysis of the reaction $Li^7(pp)$ is complicated by the fact that the ground state of Li^7 has non-zero angular momentum. This fact also means that, except in the case where the relative angular momentum ℓ of the effective incident proton waves is zero, a coupling scheme by which one can arrive at a given total angular momentum state of the compound nucleus is not unique. Since the angular distribution of the scattered protons depends on the type of

coupling, one expects an analysis of experimental data to provide information about the coupling of angular momentum vectors in the nucleus. If one specifies the type of coupling exactly, as Russell-Saunders coupling, a definite angular distribution of the reaction products is expected. The question of coupling may be sidestepped by introducing the channel spin S, which is the vector sum of the spin s of the incident particle and the total angular momentum I of the target nucleus. For an incident particle with $s = 1/2$, S has two values, $|I - s|$ and $I + s$. The contributions of the two channels to the formation of a given compound state of total angular momentum J are independent, and the theoretical angular distribution of the reaction products may be expressed in terms of an additional parameter, the mixing ratio t, which represents the ratio of the contribution of channel spin S_1 to that of channel spin S_2. This parameter is then evaluated experimentally.

The angular momentum of the ground state of Li^7 is known to be 3/2, and its parity is generally assumed to be odd. The spin of the proton is 1/2, and its parity is taken as even. The available channel spins are therefore $S = 1, 2$, and the channel parities are odd. Incident proton waves with $\ell = 0$ can form only compound states with $J = S$, odd parity, and there is no arbitrariness in the coupling scheme. However, incident proton waves with $\ell = 1$ can form compound states with $J = 0$ from channel spin 1, states with $J = 1$ and $J = 2$ from both channels, and states with $J = 3$ from channel spin 2, all with even parity. The nonexistence of alpha particles corresponding

to the 441 kev Li^7 (p γ) resonance enables one to assume that the related state in Be^8 does not have both even angular momentum and even parity, consequently we need be concerned only with the possibility that this state has J = 1 or 3, if it is formed by p-wave protons.

A preliminary theoretical analysis of the present data has been performed, using the single-level formulation given by Cohen[9]. Some of the theoretical curves for the angular variation of the maximum ratio of elastic scattering cross section to Rutherford cross section near 441 kev are plotted in Figure 12, with the experimental values included for reference. The best fit to the data is obtained by assuming a J = 1, even parity, state in Be^8 formed by p-wave protons, with a mixing ratio t = 1/2 between channel spin 1 and channel spin 2. In this case the theoretical angular distributions of the associated gamma rays are $1 + 0.16 \cos^2 \theta$ for the 17.6 Mev radiation and $1 + 0.015 \cos^2 \theta$ for the 14.8 Mev radiation. The fit if one assumes a mixing ratio t = 1/5, which corresponds to the "LS" assignment $^3S_1$ and which is necessary to explain the isotropy of the gamma radiation found by Devons and Hine[7], is not quite so good; but this possibility is certainly not excluded. A more rigorous theoretical treatment would undoubtedly be advantageous. However, it seems clear that the possibility that the state is formed by s-wave protons is definitely excluded.

Near 1030 kev, the differential cross section results for scattering angles greater than 100 degrees are consistent with spherical symmetry, which indicates that the reaction is induced by s-wave protons. Single-level theoretical curves for the angular variation

of the change in magnitude of the ratio of the cross section to Rutherford near 1030 kev, assuming $\ell = 0$, are plotted in Figure 13. The fit to the data of the curve for J = 1 is good qualitatively, and within about 25 per cent quantitatively. The effects of broad resonances above 1 Mev and the influence of competing reactions, both of which are neglected in the present theoretical treatment, can easily be blamed for the lack of quantitative fit. Again a more rigorous theoretical treatment would be advantageous.

In conclusion, the results of this experiment indicate that the 17.62 Mev level in Be^8 has J = 1, even parity, and is formed from Li^7 by p-wave protons. The 18.14 Mev state has J = 1, odd parity, and is formed by s-wave protons.

V. THE STOPPING CROSS SECTION FOR PROTONS IN LITHIUM

It can be seen from the preceding sections that, with the experimental methods outlined, the accuracy with which a scattering cross section can be measured is no better than the accuracy with which the stopping cross section for the scattered particle in the target material is known. The stopping cross section for protons in lithium metal was given in 1938 by Haworth and King[16] for proton energies from 35 - 400 kev. They compared their results with the theoretical expression of Livingston and Bethe[17], and found the value I = 32 ev for the average ionization potential of lithium metal. Their experiment was performed by comparing thick and thin target yields, making use of the ratio of the stopping cross section of lithium to that of air given by Mano[18]. Their result differed somewhat from the value I = 38 ev given by Mano for alpha particles in lithium.

Since no measurements had been made in the energy range of interest in these experiments, it was decided to measure the relative stopping cross section for protons in lithium over this range. By normalizing the results to the theory at higher energies, the correct shape of the curve over the range of interest could then be determined. It was also hoped that the quality of the fit to the theory over the entire energy range measured would give an indication of the accuracy of the assumed value for I in the theory.

1. Experimental Procedure.

The method used was extremely simple. The equipment was first calibrated at several bombarding energies by measuring the energy of protons scattered from the surface of a clean copper target. A very thin layer of lithium was then deposited on the copper, and the measurements repeated. The proton energy lost in passing through the lithium layer before and after being scattered by the copper could therefore be determined.

This work was performed at a scattering angle of 130 degrees. The scattering from clean copper was done at ion energies of 450 and 1000 kev, using the H^+ and HHH^+ beams. This experiment checked the previous calibration of the apparatus and indicated that the calibration was linear within 0.1 per cent, allowing the scattered proton energies to be calculated confidently at other bombarding energies. The thin lithium layer was then deposited, and the energy loss measured for bombarding ion energies of 450, 600, 800, 1000 and 1350 kev, using the H^+ and HHH^+ beams.

2. Calculations and Results.

Assume a beam of protons incident on the target with energy E_{1B}. If the target is copper alone, protons scattered from the surface will have energy E_{2B} where $E_{2B} = \alpha(Cu)\, E_{1B}$. $\alpha(Cu)$ is given by equation 3.12a, in which M is now the mass of a copper nucleus. If the target is lithium on copper, the protons lose

energy ΔE_1 while traveling inward through the lithium and energy ΔE_2 while escaping from the layer after being scattered; so those scattered at the copper surface enter the spectrometer with energy E_{2o}, where

$$E_{2o} = \alpha(Cu)\ (E_{1B} - \Delta E_1) - \Delta E_2.$$

Protons scattered by the thin lithium layer during transit will have energies much less than E_{2o} since more energy is taken by the recoil of the light lithium nuclei than by the recoil of the heavier copper nuclei. Consequently these protons are not accepted by the spectrometer. The energy losses ΔE_1 and ΔE_2 in the layer may be expressed in terms of the stopping cross section of lithium, so that

$$\Delta E_1 = N_s \frac{x}{\cos \theta_1} \varepsilon(\bar{E}_1)$$

$$\Delta E_2 = N_s \frac{x}{\cos \theta_2} \varepsilon(\bar{E}_2)$$

where x is the thickness of the lithium layer, and $\bar{E}_1$ and $\bar{E}_2$ are some intermediate energies in the layer of the incoming and outgoing beams, respectively. Thus, if the target is set so that $\theta_1 = \theta_2$, the measured energy loss due to the presence of thelithium layer is

$$\delta E_{2o} = E_{2B} - E_{2o} = a\Delta E_1 + \Delta E_2 \qquad (5.1)$$

$$= N_s \frac{x}{\cos \theta_1} [a\varepsilon(\bar{E}_1) + \varepsilon(\bar{E}_2)],$$

where a is $a(Cu)$.

Expanding $\varepsilon(\bar{E}_1)$ and $\varepsilon(\bar{E}_2)$ about some energy E_x, we obtain

$$\delta E_{2o} = N_s \frac{x}{\cos \theta_1} \left\{ (a+1)\, \varepsilon(E_x) + \frac{d\varepsilon}{dE}\bigg|_{E=E_x} [a\bar{E}_1 + \bar{E}_2 - (a+1)E_x] \right.$$

$$\left. + \frac{1}{2} \frac{d^2\varepsilon}{dE^2}\bigg|_{E=E_x} [a(\bar{E}_1 - E_x)^2 + (\bar{E}_2 - E)_x^2] + \cdots \right\}$$

Setting $E_x = \dfrac{a\bar{E}_1 + \bar{E}_2}{a+1}$ to eliminate the first order term, we have

$$\delta E_{2o} = N_s \frac{x}{\cos \theta_1} \left\{ (a+1)\, \varepsilon\left(\frac{a\bar{E}_1 + \bar{E}_2}{a+1}\right) \right.$$

$$\left. + \frac{1}{2} \frac{d^2\varepsilon}{dE^2}\bigg|_{E=E_x} \frac{a}{a+1} (\bar{E}_1 - \bar{E}_2)^2 + \cdots \right\} . \qquad (5.2)$$

To determine $\bar{E}_1$ and $\bar{E}_2$ we set $\varepsilon(E) = C/E^{a(E)}$. Over a small energy variation, $a(E)$ remains essentially constant so that taking $a(E_1) = a_1$, and $a(E_2) = a_2$, we may write

$$N_s \frac{x}{\cos \theta_1} = \frac{\Delta E_1}{\varepsilon(\bar{E}_1)} = \int_{E_{1B}-\Delta E_1}^{E_{1B}} \frac{dE}{\varepsilon(E)}$$

so that

$$\Delta E_1 \, \bar{E}_1^{a_1} = \int_{E_{1B}-\Delta E_1}^{E_{1B}} E^{a_1} \, dE = \frac{1}{a_1 + 1} \left[E_{1B}^{a_1+1} - (E_{1B} - \Delta E_1)^{a_1+1} \right].$$

Solving for $\bar{E}_1$ we obtain

$$\bar{E}_1 = E_{1B} \left[1 - \frac{1}{2} \frac{\Delta E_1}{E_{1B}} + \frac{1}{24} (a_1 - 1) \left(\frac{\Delta E_1}{E_{1B}} \right)^2 + \cdots \right] \tag{5.3}$$

and similarly for $\bar{E}_2$ we obtain

$$\bar{E}_2 = E_{2o} \left[1 + \frac{1}{2} \frac{\Delta E_2}{E_{2o}} + \frac{1}{24} (a_2 - 1) \left(\frac{\Delta E_2}{E_{2o}} \right)^2 + \cdots \right] \tag{5.4}$$

If we ignore the second-order terms in equations 5.3 and 5.4, and use equation 5.1, we may now write

$$E_x = \frac{a\bar{E}_1 + \bar{E}_2}{a + 1} = \frac{E_{2B} + E_{2o}}{a + 1} + \frac{\delta E_{2o}}{2(a + 1)} \cdot \frac{\frac{\Delta E_2}{\Delta E_1} - a}{\frac{\Delta E_2}{\Delta E_1} + a} .$$

The second term of this expression was found to be about 2 per cent of the first term; so the second term was evaluated by setting $\frac{\Delta E_2}{\Delta E_1} = \frac{\varepsilon(E_{2o})}{\varepsilon(E_{1B})}$ and taking values for $\varepsilon(E_{2o})$ and $\varepsilon(E_{1B})$ from the theoretical stopping cross section curve. The effect of the second-order terms in equations 5.2, 5.3 and 5.4 was investigated

by successive approximation and found to be entirely negligible for the accuracy attainable in this experiment. The expression used in calculating the final results was therefore

$$\varepsilon\left(\frac{E_{2B}+E_{2o}}{\alpha+1}+\frac{E_{2B}-E_{2o}}{2(\alpha+1)}\,\frac{\eta'-\alpha}{\eta'+\alpha}\right)=\frac{E_{2B}-E_{2o}}{B}$$

where $B = N_s \frac{x(\alpha+1)}{\cos\theta_1}$ and was a constant of the target angle and of the particular lithium layer, and where $\eta' = \frac{\varepsilon(E_{2o})}{\varepsilon(E_{1B})}$.

The constant B was evaluated by normalizing the experimental results to the theoretical expression of Livingston and Bethe at a single point, E = 951.7 kev, using the value I = 32 ev given by Haworth and King. The fit of the remaining experimental points to the theory is shown in Figure 11. It can be seen that the fit is very good over the energy range studied, indicating that the theoretical expression is valid over this range. The theoretical curve with I = 32 ev was therefore used in calculating the Li^7 (pp) cross sections. The relative values measured in this experiment, which should be accurate to 3 per cent, are given in Table 9 in terms of the value at 951.7 kev.

After this work was completed, it was pointed out to the author that recently an absolute determination of I for lithium has been made by Bakker and Segre'[19], who give I = 34.0 ev within about 10 per cent. This is seen to be in agreement with the result of Haworth and King. Since a difference of 2 ev in I makes a

difference of about 2 per cent in the lithium stopping cross section, this agreement in conjunction with the results of the present experiment indicates that the uncertainty introduced into the $Li^7(pp)$ cross sections by the use of the I = 32 ev theoretical stopping cross section curve is of the order of 5 per cent.

TABLE 9

The stopping cross section of protons in lithium metal at various energies, referred to the value at 951. 7 kev.

E(kev)	$\frac{\varepsilon(E)}{\varepsilon(951.7)}$
209.0	2.58
280.3	2.27
387.7	1.86
404.0	1.81
404.3	1.79
558.9	1.43
760.3	1.17
951.7	1.00
1299.2	0.865

APPENDIX I.

CORRECTION FOR SCATTERING FROM Li^6 AT FORWARD ANGLES.

Since natural lithium metal was used for the targets in this experiment, Li^6 was present in its natural abundance, i.e., 0.075. The high resolution of the spectrometer made it possible to separate the protons scattered by Li^7 from those scattered by Li^6 at scattering angles greater than 80 degrees. However, at more forward angles particles scattered by both isotopes were counted and a correction to the observed cross section was necessary.

Let us denote the two isotopes, of abundances A and A*, by unstarred and starred symbols, respectively. If the detector were able to differentiate between particles scattered by one or the other isotope we would have, from equation 3.11, at given values of the bombarding energy and spectrometer setting,

$$\frac{d\sigma}{d\Omega}(E_1, \theta) = \frac{N_s}{N} \frac{ZeR}{2CVE_{2o}} (\alpha + \eta)\, \varepsilon(E_1)\, n_p(E_1, \theta)$$

$$\frac{d\sigma^*}{d\Omega}(E_1^*, \theta) = \frac{N_s}{N^*} \frac{ZeR}{2CVE_{2o}} \varepsilon(E_1^*)\, (\alpha^* + \eta^*)\, n_p^*(E_1^*, \theta)$$

where $\frac{N}{N_s} = A$, and $\frac{N^*}{N_s} = A^*$. E_1 and E_1^* are the reaction energies corresponding to E_{1B} and E_{2o} (equation 3.7). However, if the detector does not differentiate between the two sets of particles it counts $N_p = n_p + n_{p^*}$. If we are interested in the cross section

of the unstarred isotope, we therefore take $n_p = N_p - n_{p^*}$. Substituting this in the above equations, we obtain for the unstarred cross section

$$\frac{d\sigma}{d\Omega}(E_1,\theta) = \frac{d\sigma_o}{d\Omega} - \frac{N^*}{N}\,\frac{(\alpha+\eta)\,\varepsilon(E_1)}{(\alpha^*+\eta^*)\,\varepsilon(E_1^*)}\,\frac{d\sigma^*}{d\Omega}(E_1^*,\theta)$$

where $d\sigma_o/d\Omega$ is the unstarred cross section as calculated from the observed number of counts.

Expressed as the ratio to Rutherford scattering, we have

$$\frac{\sigma}{\sigma_R} = \frac{\sigma_o}{\sigma_R} - \frac{N^*}{N}\,\frac{(\alpha+\eta)\,\varepsilon(E_1)}{(\alpha^*+\eta^*)\,\varepsilon(E_1^*)}\,\frac{\sigma^*(E_1^*,\theta)}{\sigma_R(E_1,\theta)}$$

For the separation of the lithium isotopes, taking Li^7 as the unstarred isotope, $N^*/N = A^*/A = 0.081$. If the scattering from Li^6 is assumed to be given by the Rutherford scattering law, the remaining factors in the correction term give a product which for this experiment was always very nearly unity. Therefore if the spectrometer accepts protons scattered by both Li^7 and Li^6, the ratio of the Li^7 scattering cross section to the Rutherford cross section is given by

$$\frac{\sigma}{\sigma_R}(E_1,\,\theta) = \frac{\sigma_o}{\sigma_R} - 0.08$$

This correction was applied to the results at $\theta_{CM} = 50$ and 70 degrees.

The Li^6 Rutherford scattering assumption was checked at

400 kev and found to be true within about 20 per cent. The results of Bashkin and Richards[15] on Li^6(pp) indicate that it is also very nearly true at 1200 kev for scattering at 166 degrees. However the presence of levels in Be^7 at proton energies near 900 kev (broad) and 1820 kev throws some doubt at other energies. Consequently the Li^7(pp) results at 50 and 70 degrees may be several per cent in error due to this cause.

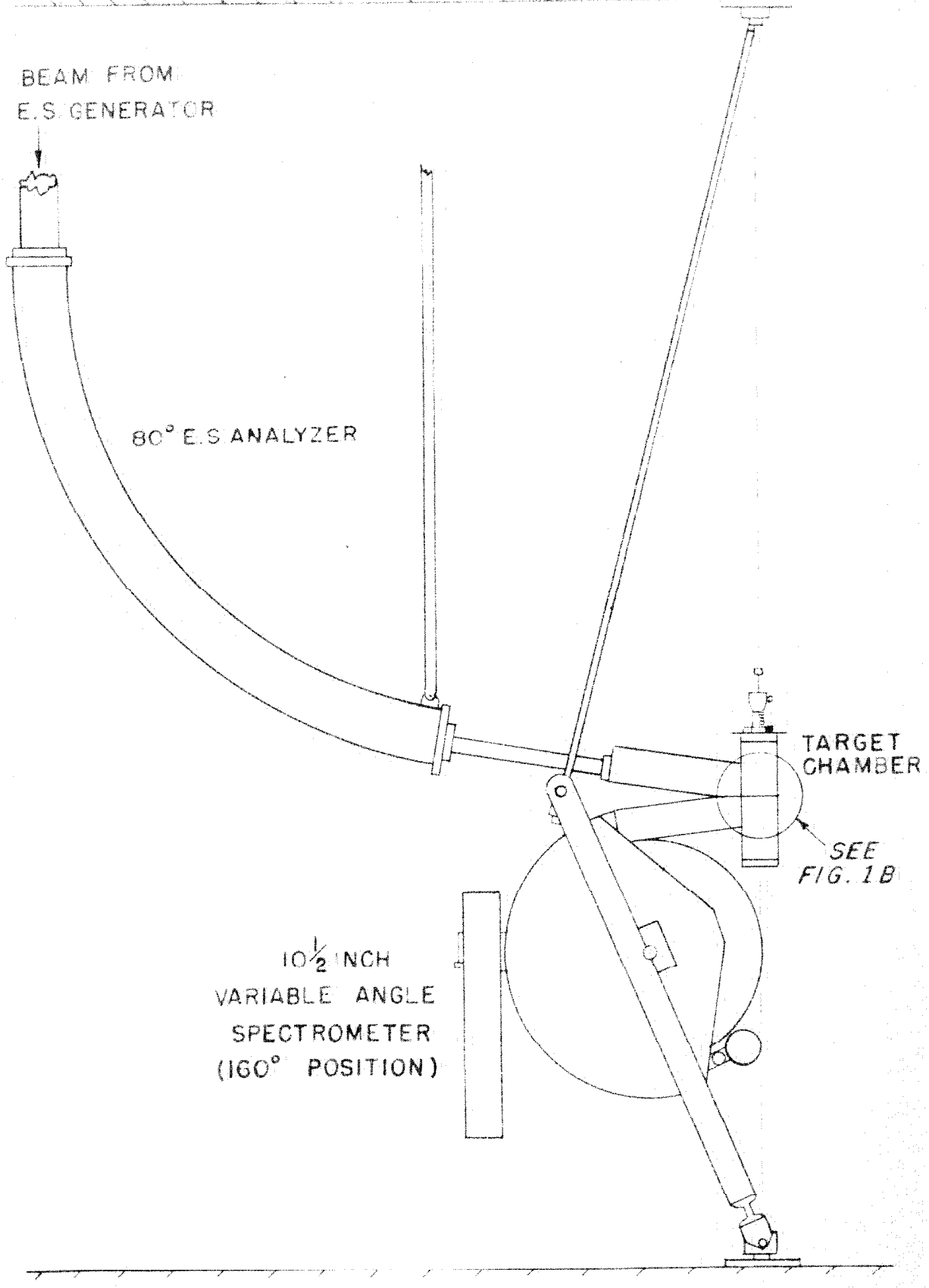

FIGURE 1A- LAYOUT OF APPARATUS

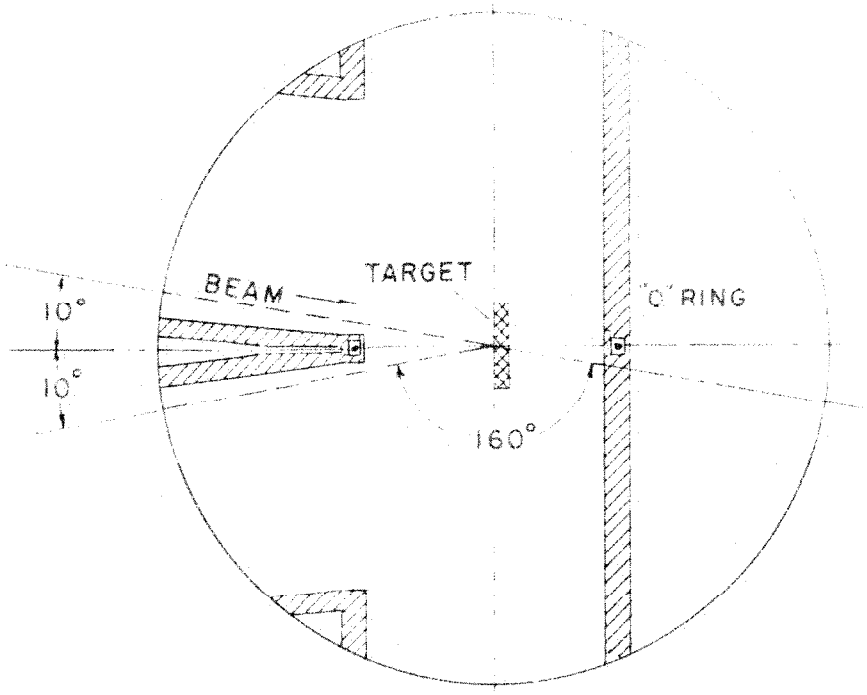

160° POSITION

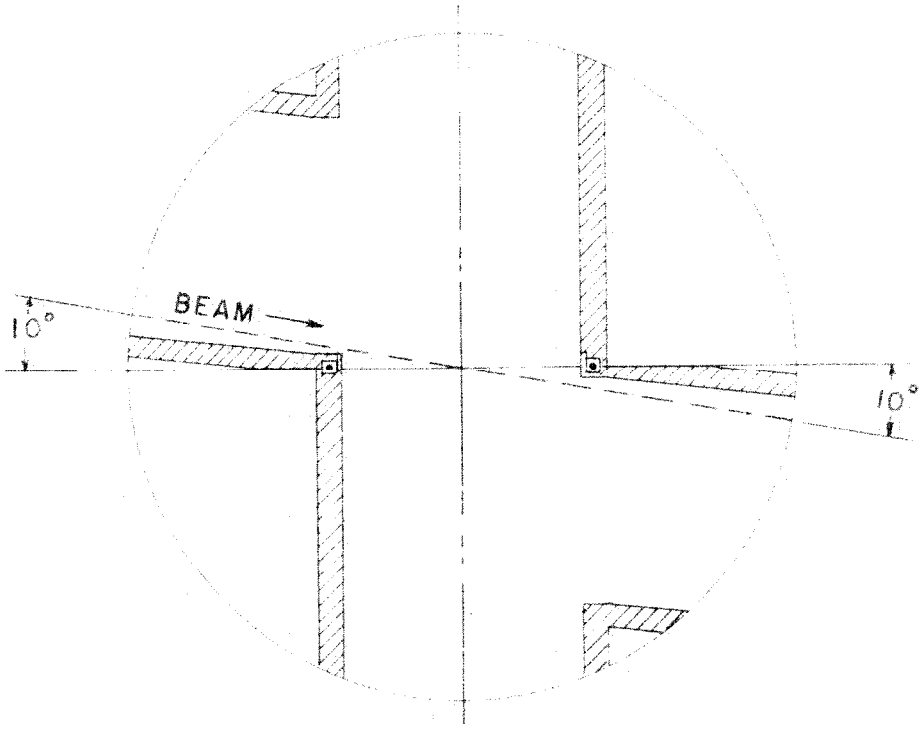

0° POSITION

FIGURE 1B - TARGET CHAMBER DETAIL

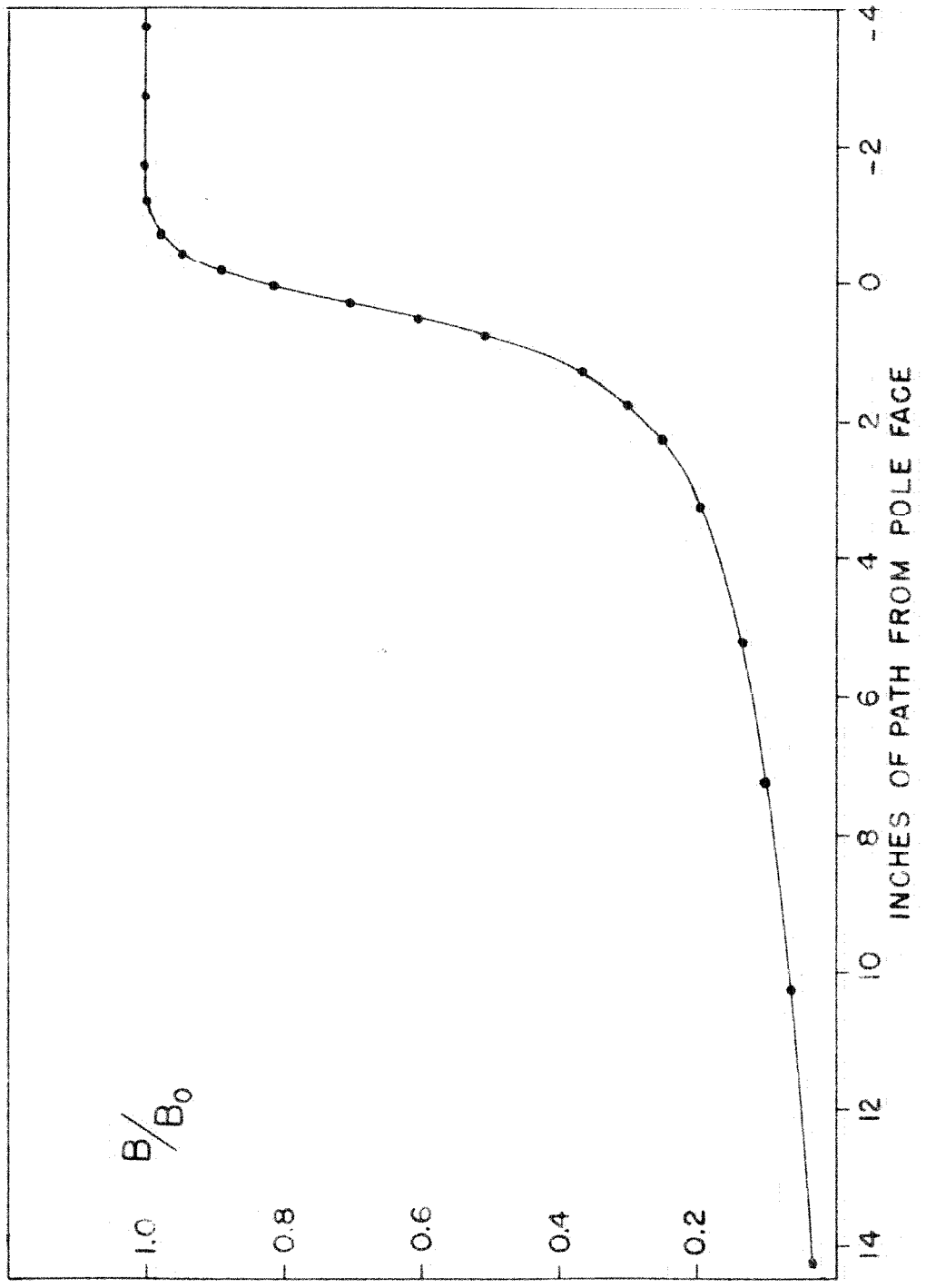
B/B₀
1.0
0.8
0.6
0.4
0.2
14
12
10
8
6
4
2
0
-2
-4
INCHES OF PATH FROM POLE FACE

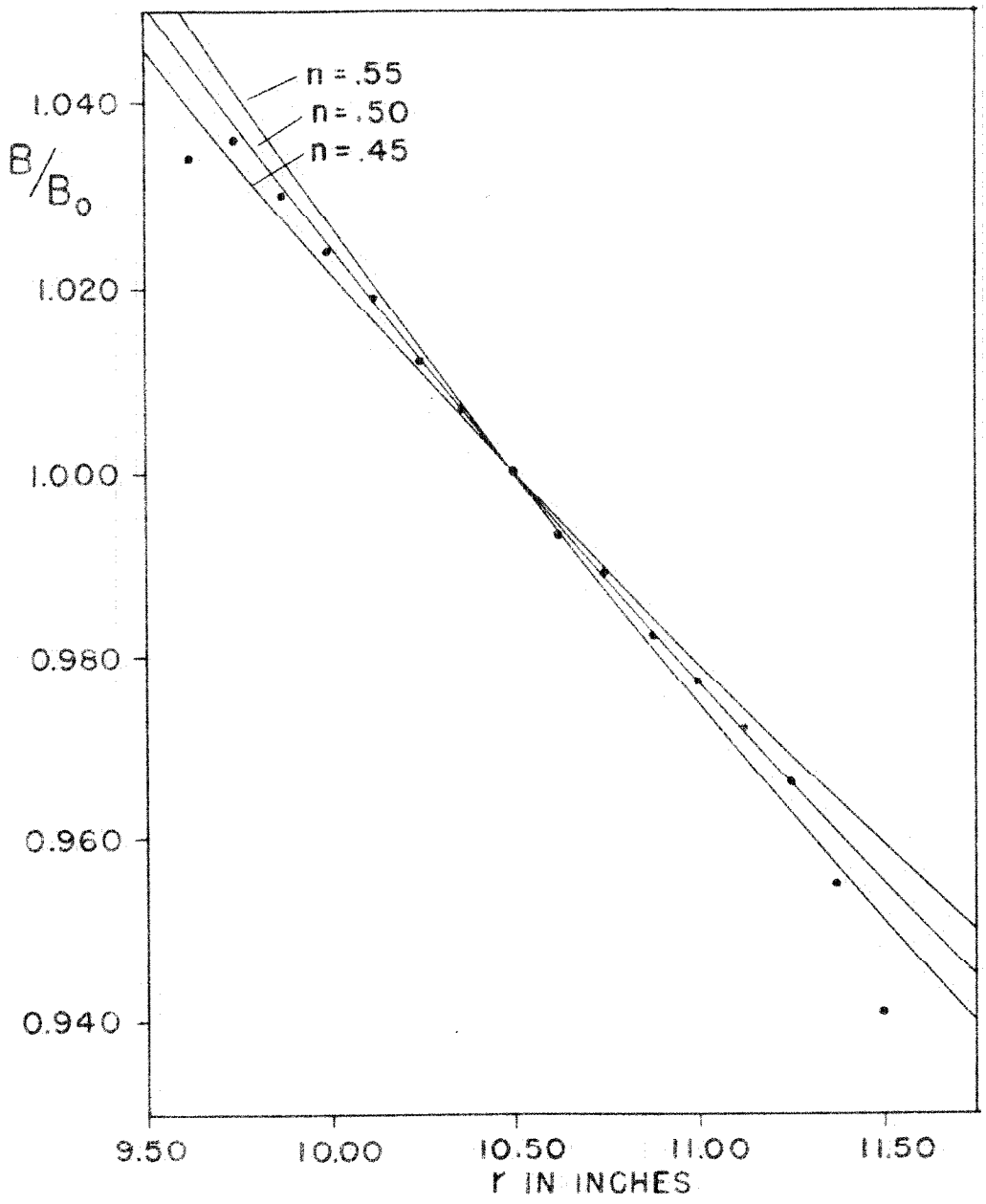
n = .55
n = .50
n = .45
B/B0
1.040
1.020
1.000
0.980
0.960
0.940
9.50
10.00
10.50
11.00
11.50
r IN INCHES

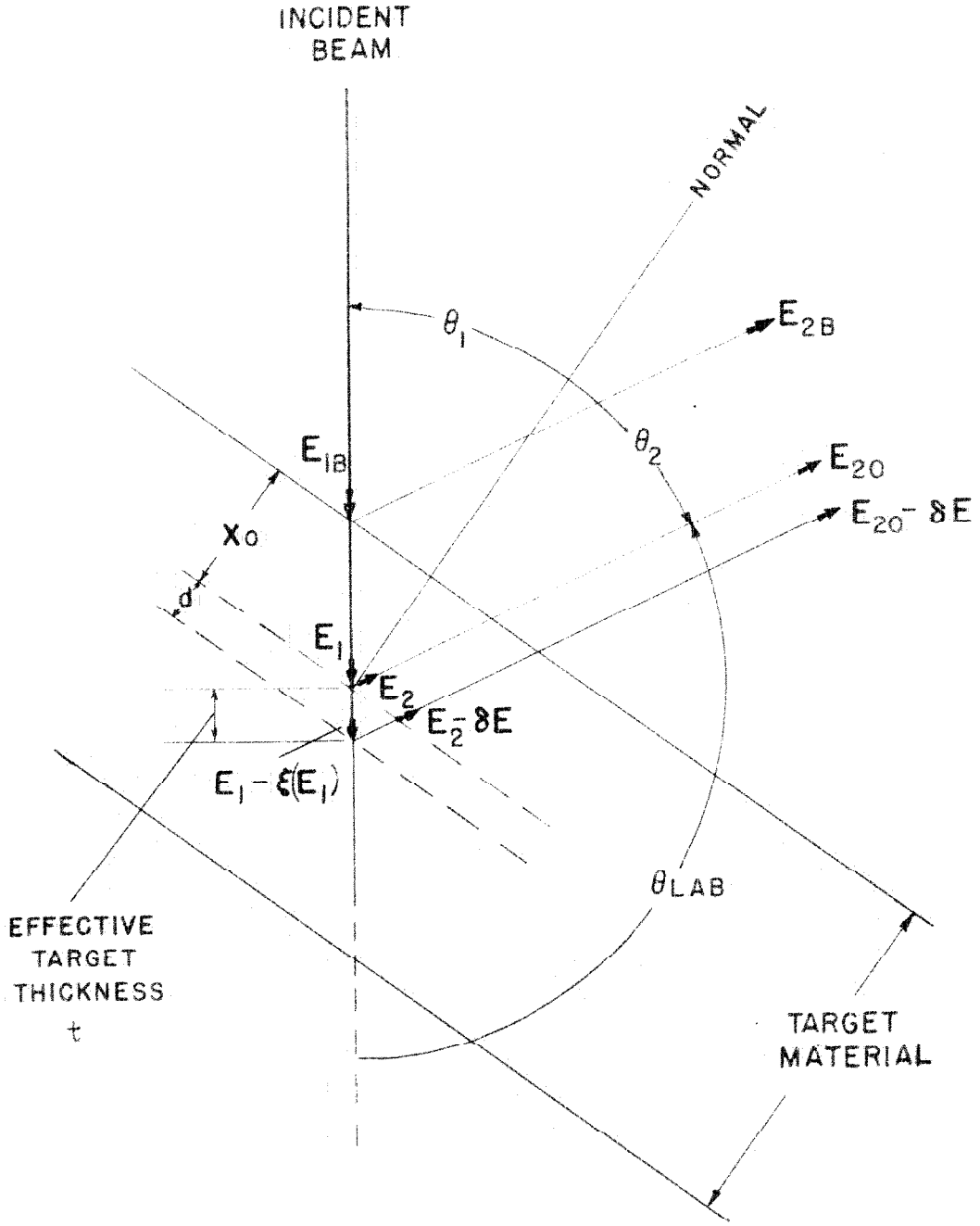

FIGURE 4

ENERGY RELATIONS IN TARGET

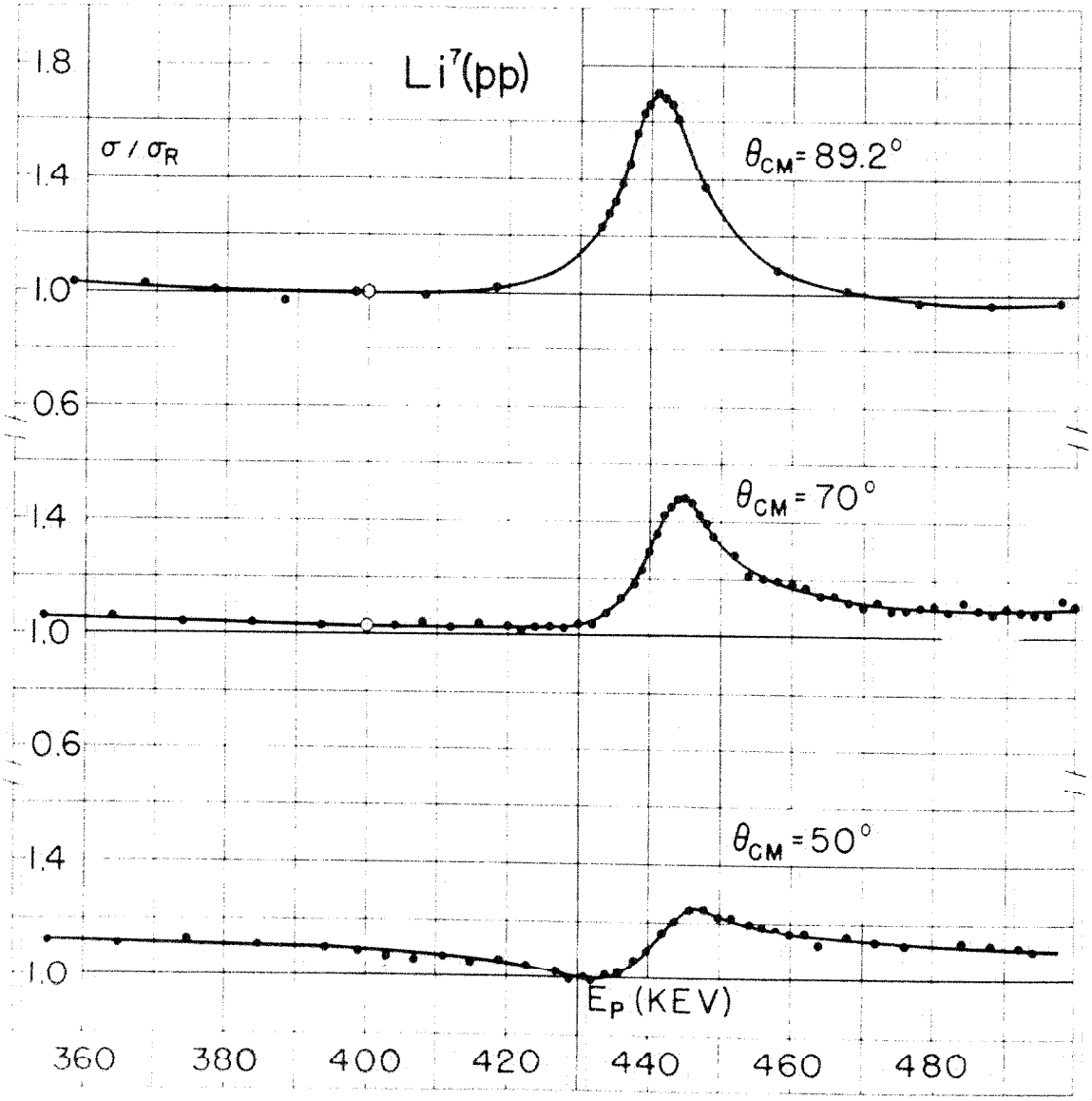
Li⁷(pp)
σ / σR
θCM = 89.2°
θCM = 70°
θCM = 50°
1.8
1.4
1.0
0.6
1.4
1.0
0.6
1.4
1.0
EP (KEV)
360
380
400
420
440
460
480

FIGURE 5

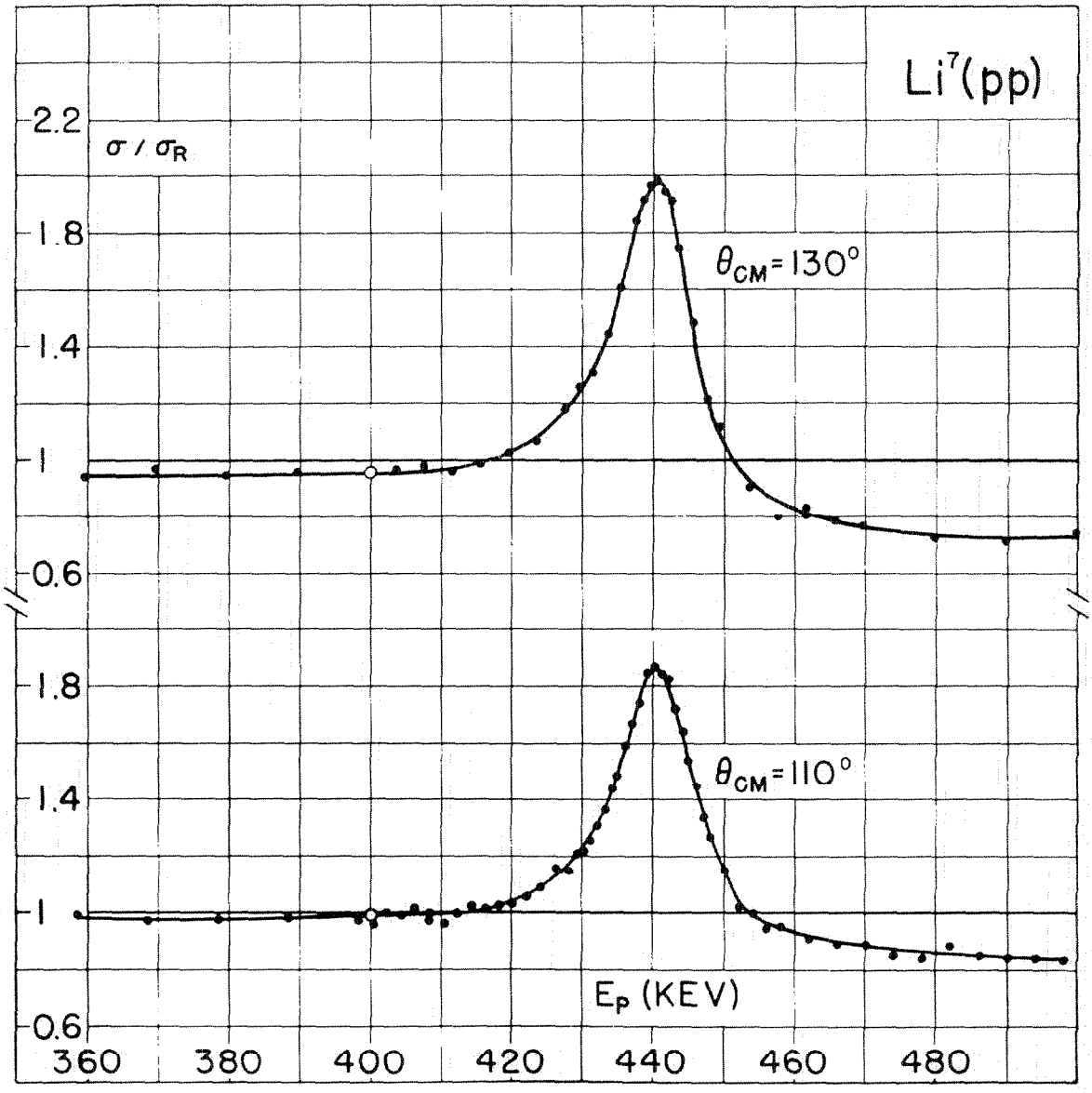
Li⁷(pp)
σ / σR
2.2
1.8
1.4
1
0.6
θCM = 130°
θCM = 110°
Ep (KEV)
360
380
400
420
440
460
480

FIGURE 6

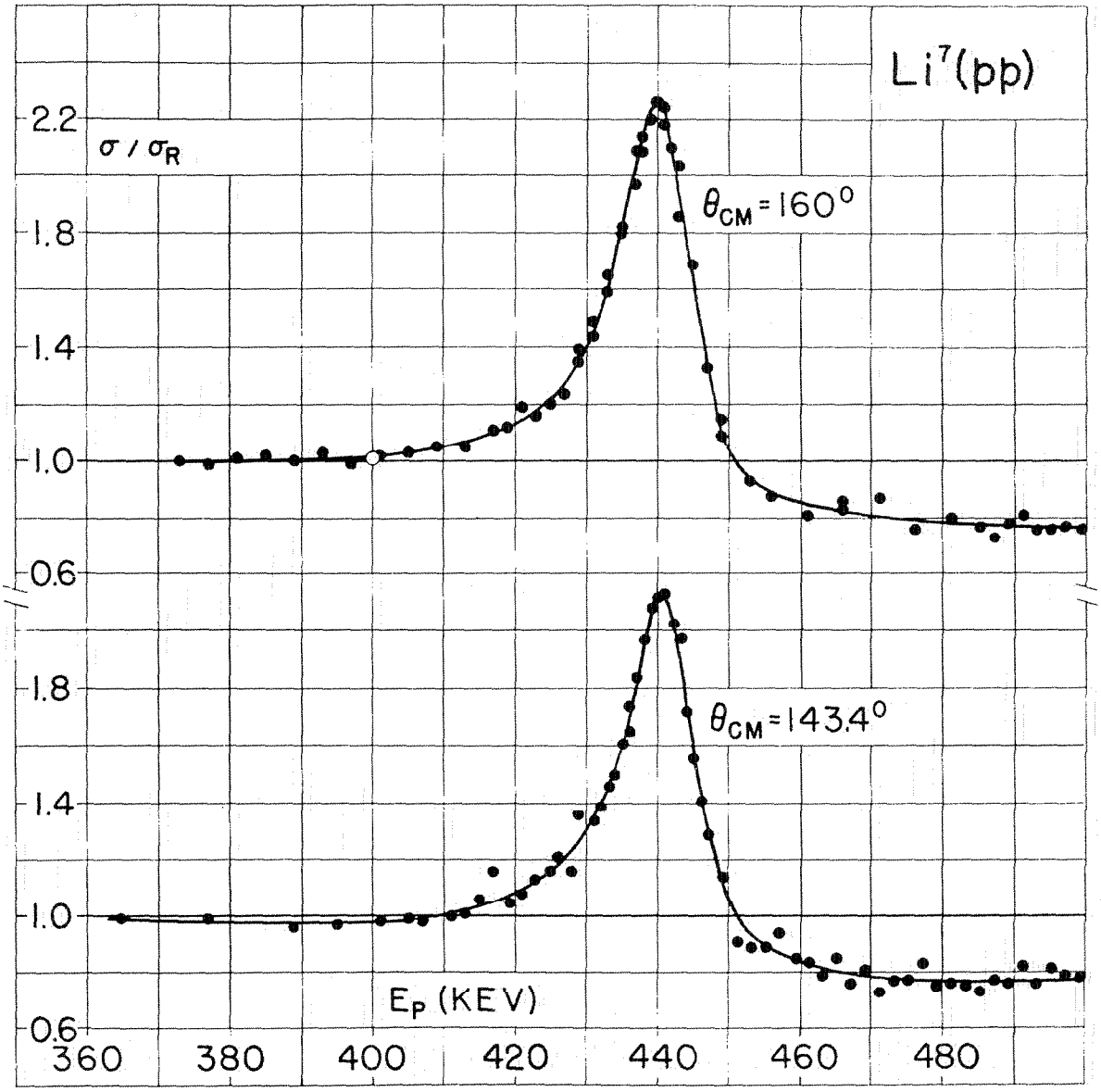
Li⁷(pp)
σ / σR
θCM = 160°
θCM = 143.4°
EP (KEV)
2.2
1.8
1.4
1.0
0.6
360
380
400
420
440
460
480

FIGURE 7

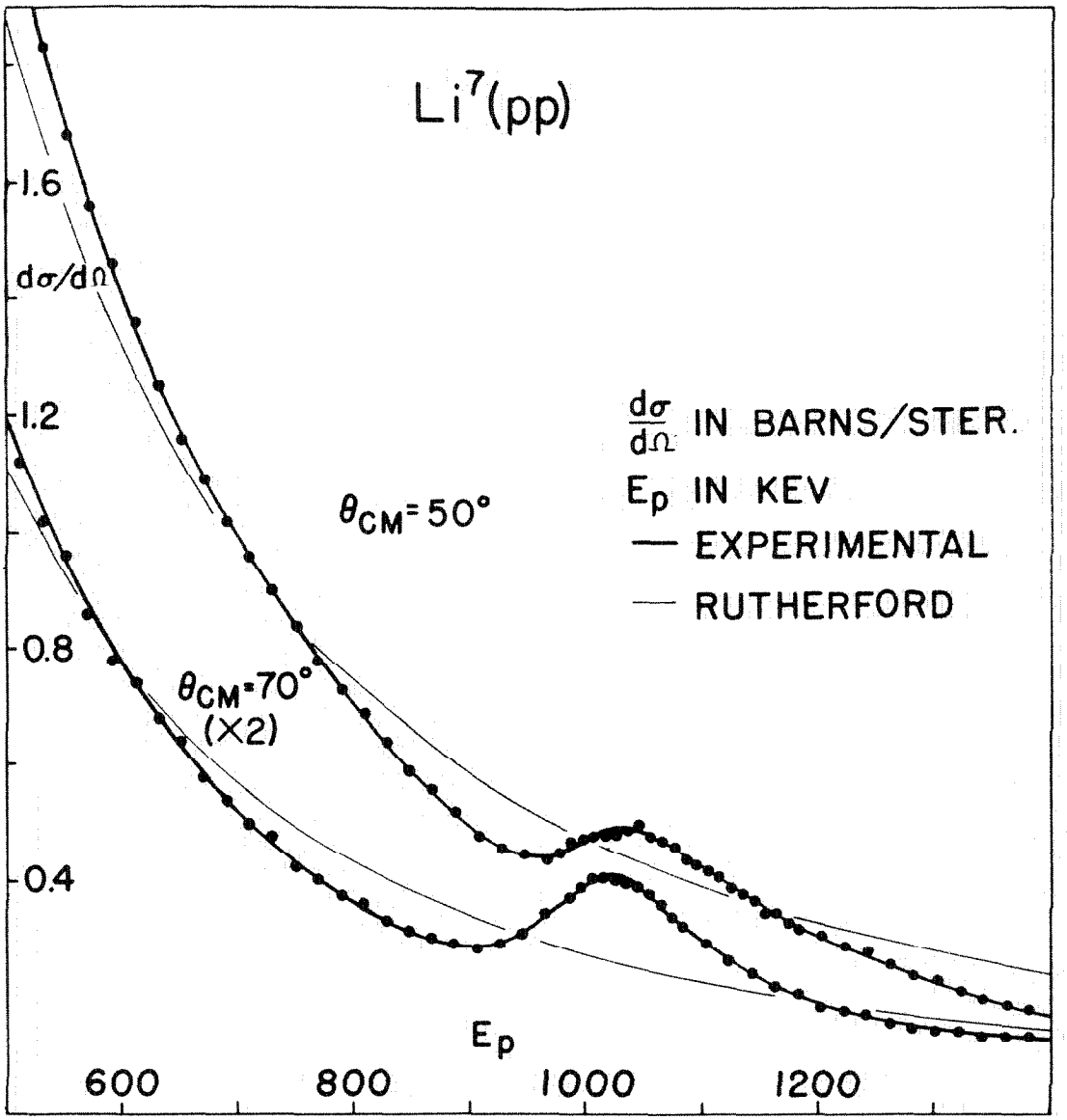
Li7(pp)
1.6
dσ/dΩ
1.2
0.8
0.4
θCM=50°
θCM=70°
(X2)
dσ/dΩ IN BARNS/STER.
Ep IN KEV
— EXPERIMENTAL
— RUTHERFORD
Ep
600
800
1000
1200

FIGURE 8

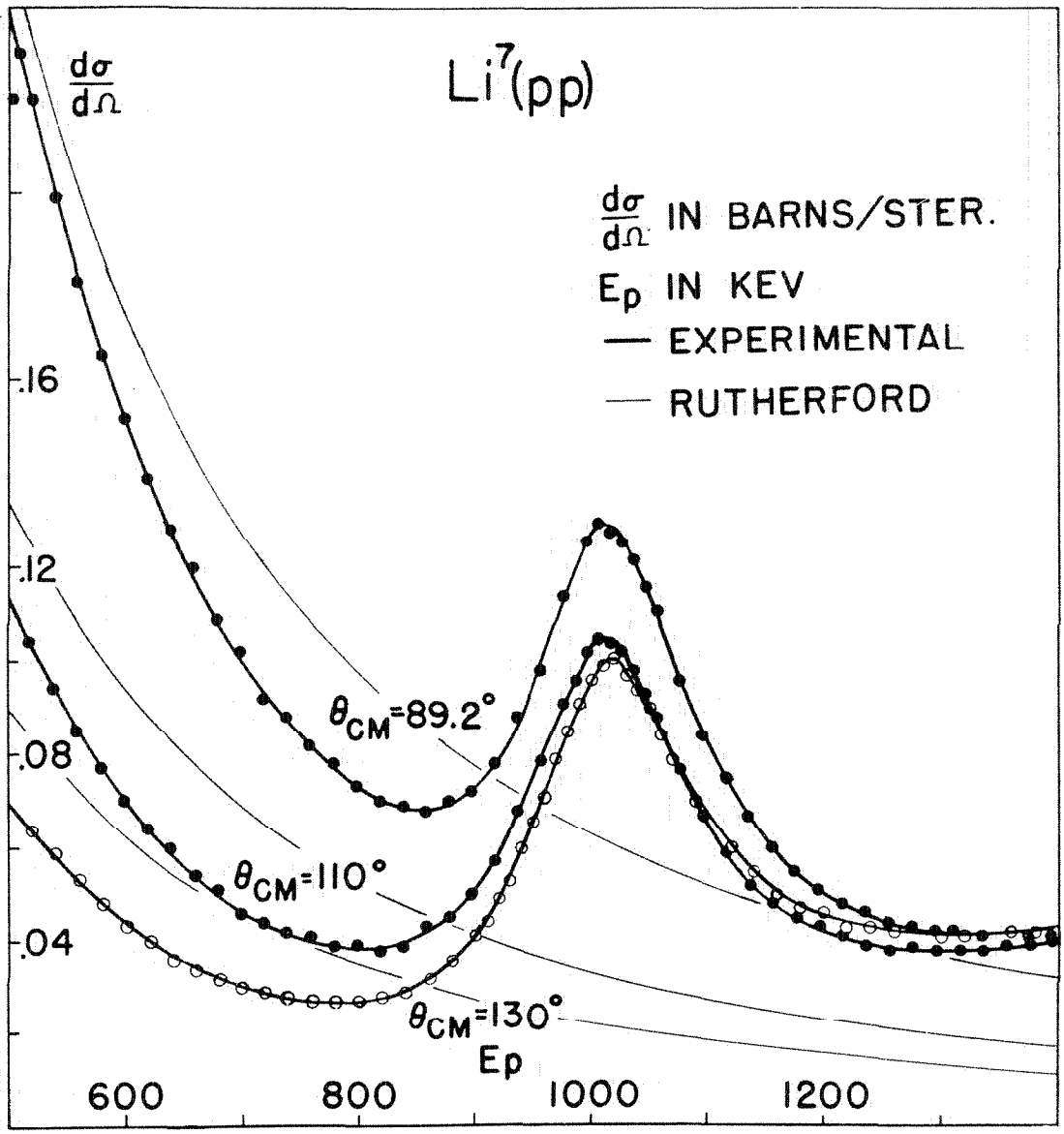
dσ/dΩ
Li⁷(pp)
dσ/dΩ IN BARNS/STER.
Ep IN KEV
— EXPERIMENTAL
— RUTHERFORD
.16
.12
.08
.04
θCM=89.2°
θCM=110°
θCM=130°
Ep
600
800
1000
1200

FIGURE 9

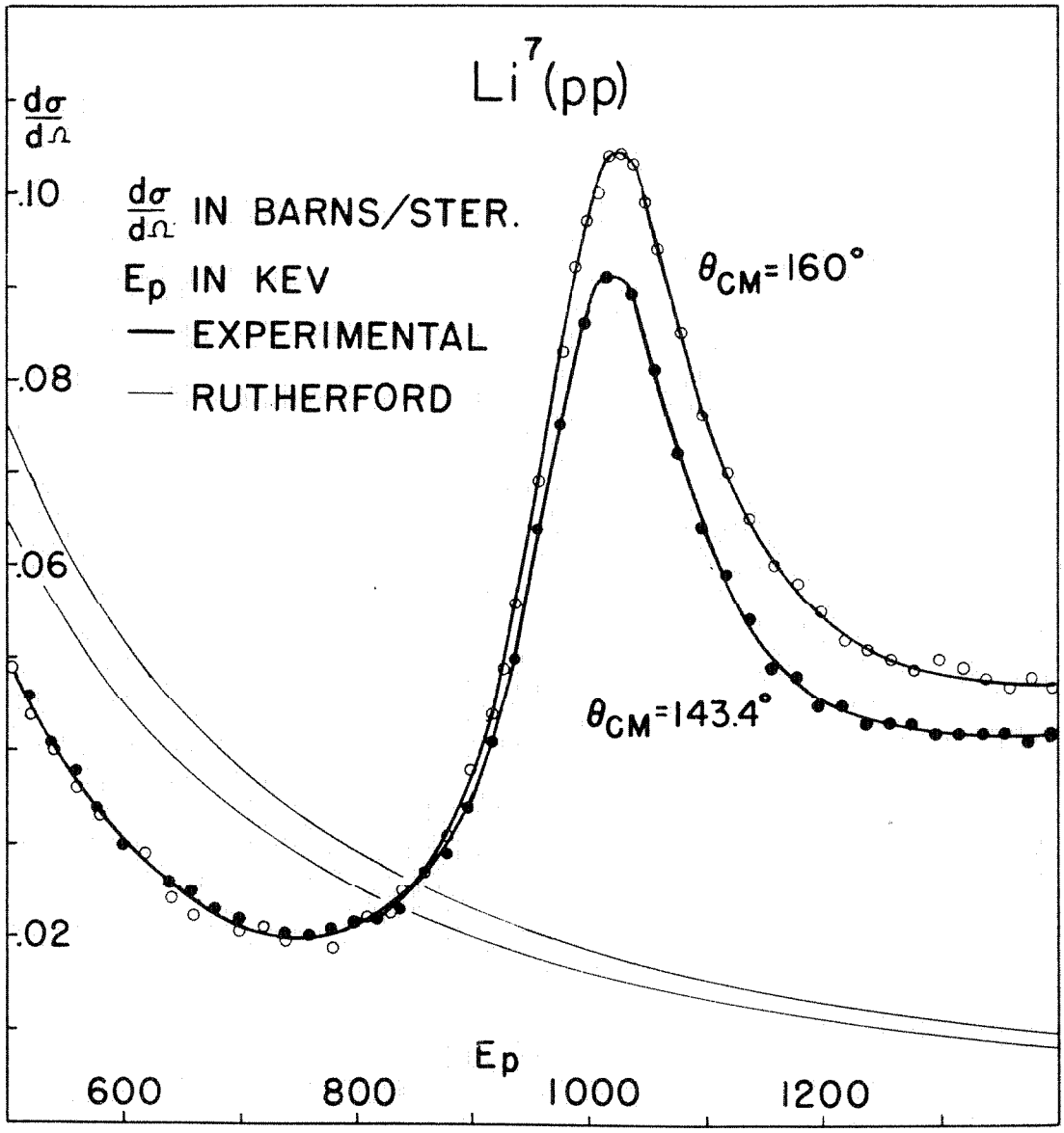
Li7(pp)
dσ/dΩ
.10
.08
.06
.02
dσ/dΩ IN BARNS/STER.
Ep IN KEV
EXPERIMENTAL
RUTHERFORD
θCM=160°
θCM=143.4°
Ep
600
800
1000
1200

FIGURE 10

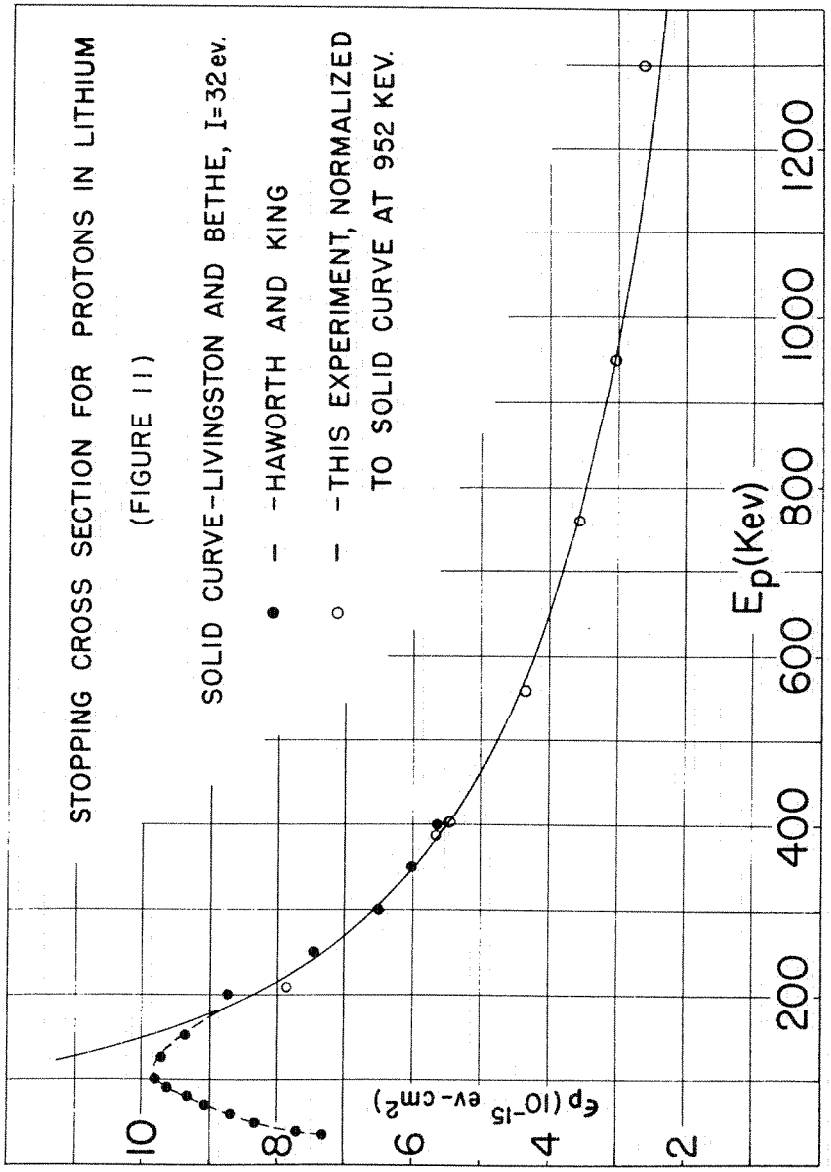
STOPPING CROSS SECTION FOR PROTONS IN LITHIUM
(FIGURE 11)
SOLID CURVE-LIVINGSTON AND BETHE, I=32 ev.
• — -HAWORTH AND KING
○ — -THIS EXPERIMENT, NORMALIZED TO SOLID CURVE AT 952 KEV.
εp (10⁻¹⁵ ev-cm²)
Ep(Kev)
10
8
6
4
2
200
400
600
800
1000
1200

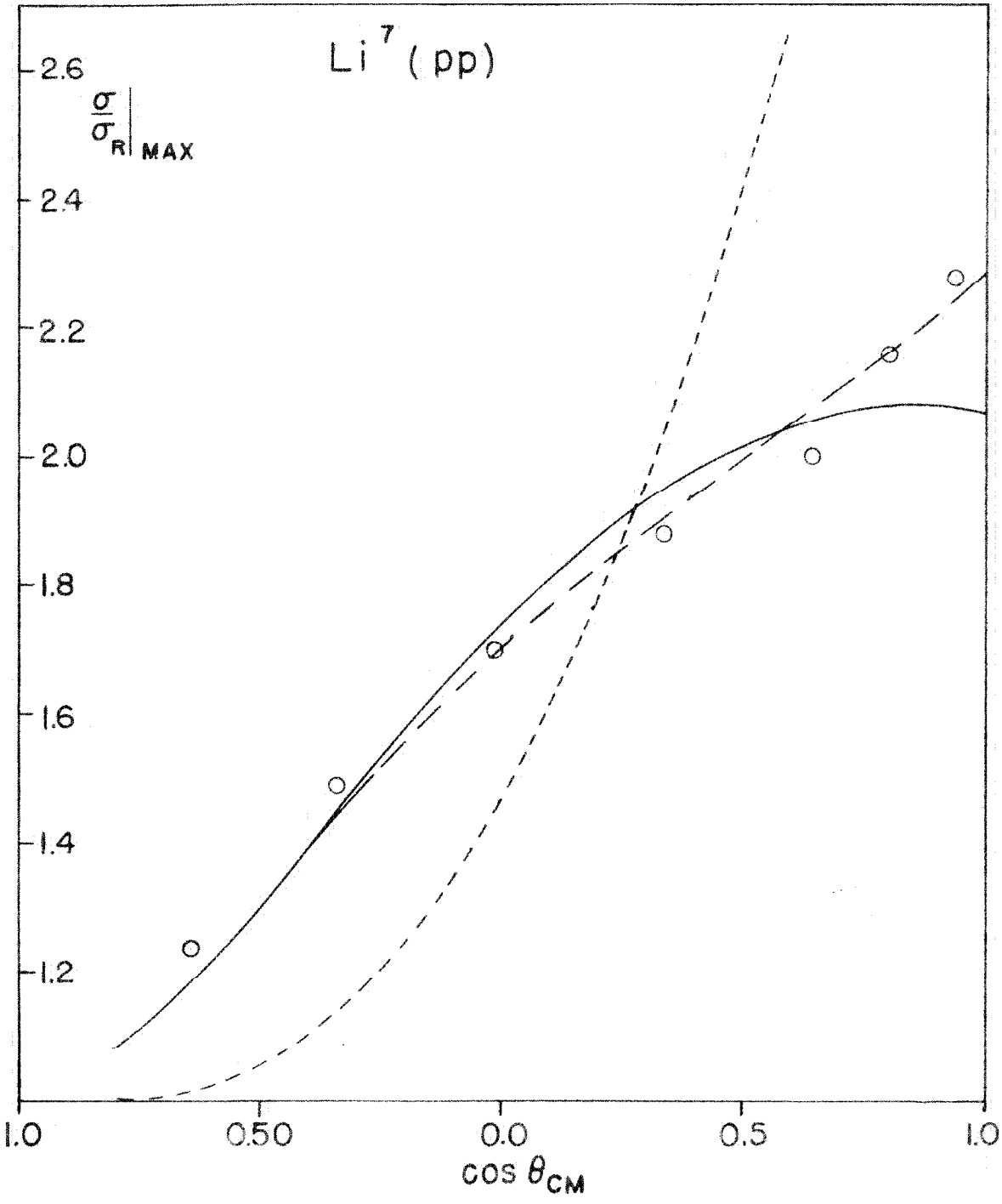
Li 7 (pp)
σ/σR| MAX
2.6
2.4
2.2
2.0
1.8
1.6
1.4
1.2
1.0
0.50
0.0
0.5
1.0
cos θCM

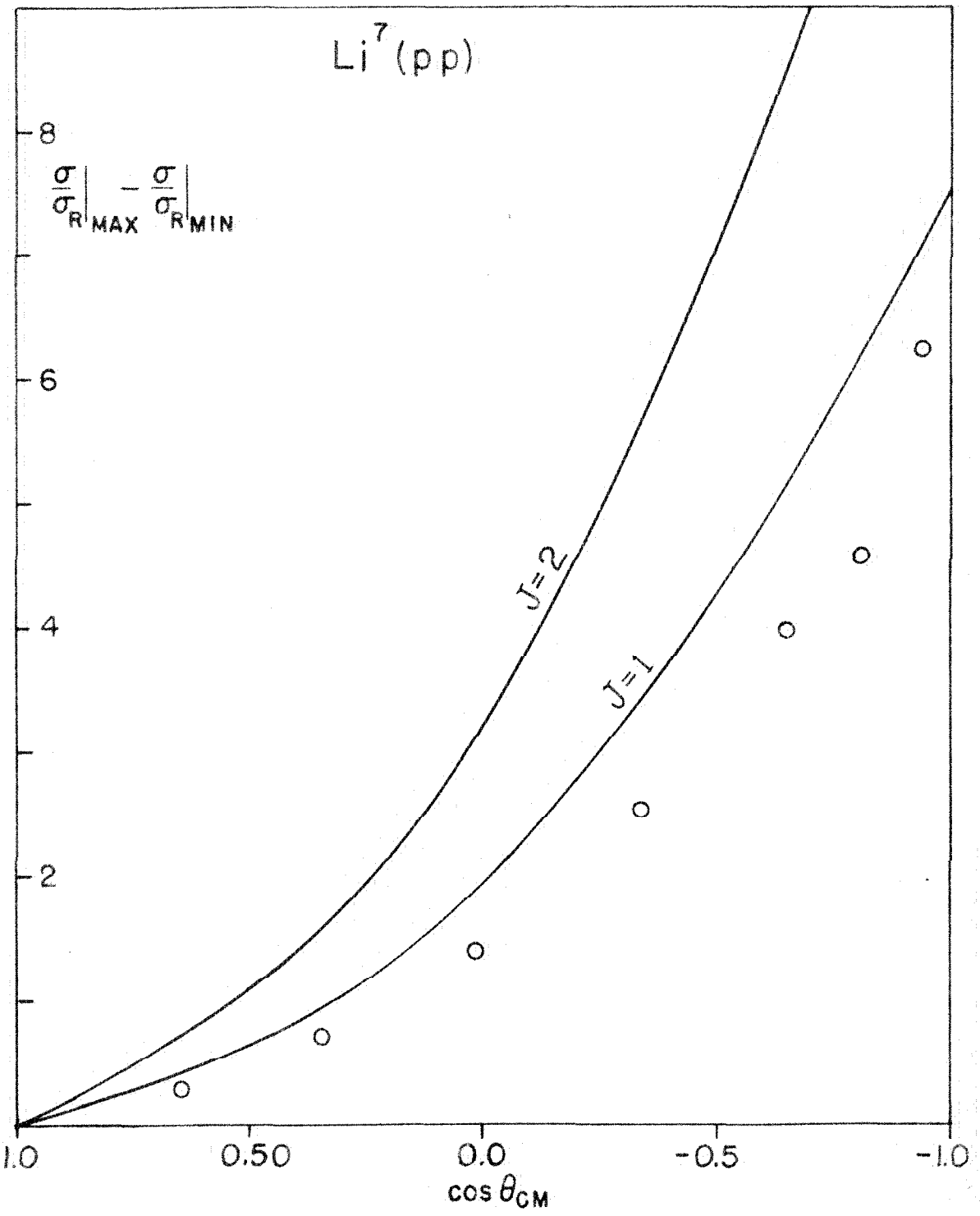
Li⁷(p p)
8
6
4
2
$\frac{\sigma}{\sigma_R}\Big|_{MAX} - \frac{\sigma}{\sigma_R}\Big|_{MIN}$
J=2
J=1
1.0
0.50
0.0
-0.5
-1.0
cos θCM

REFERENCES

(1) Cockroft, J.D. and E.T.S. Walton, Proc. Roy. Soc. 137A, 229 (1932).

(2) Lauritsen, C.C. and H.R. Crane, Phys. Rev. 45, 63 (1934).

(3) Hafstad, L.R. and M.A. Tuve, Phys. Rev. 47, 506 (1935).

(4) Creutz, E., Phys. Rev. 55, 819 (1939).

(5) Fowler, W.A. and C.C. Lauritsen, Phys. Rev. 76, 314 (1949).

(6) Hunt, S.E., Proc. Phys. Soc., A, 65, 982 (1952).

(7) Devons, S. and M.G.N. Hine, Phys. Rev. 74, 976 (1948); Proc. Roy. Soc. 199A, 56, 73 (1949).

(8) Brown, Snyder, Fowler and Lauritsen, Phys. Rev. 82, 159 (1951).

(9) Cohen, E.R., Ph. D. Thesis, California Institute of Technology, (1949).

(10) Snyder, Rubin, Fowler and Lauritsen, Rev. Sci. Inst. 21, 852 (1950).

(11) Tollestrup, A.V. Ph. D. Thesis, California Institute of Technology, (1950).

(12) Milne, E.A., Ph. D. Thesis, California Institute of Technology, (1953).

(13) Herb, Snowdon and Sala, Phys. Rev. 75, 246 (1949).

(14) Warshaw, S.D. Phys. Rev. 76, 1759 (1949).

(15) Bashkin, S. and H.T. Richards, Phys. Rev. 84, 1124 (1951).

(16) Haworth, L.J. and L.P.D. King, Phys. Rev. 54, 48 (1938).

(17) Livingston, M.S. and H.A. Bethe, Rev. Mod. Phys. 9, 261 (1937).

(18) Mano, G. Ann. de Phys. 1, 525 (1934); J. de Phys. et Rad. 5, 628 (1934).

(19) Bakker, C.J. and E. Segrè, Phys. Rev. 81, 489 (1951).